

Electrical conductivity of a warm neutron star crust in magnetic fields

Arus Harutyunyan* and Armen Sedrakian†

Institute for Theoretical Physics, J. W. Goethe University, D-60438 Frankfurt-Main, Germany

(Received 28 May 2016; revised manuscript received 9 July 2016; published 24 August 2016)

We study the electrical conductivity of finite-temperature crust of a warm compact star which may be formed in the aftermath of a supernova explosion or a binary neutron star merger as well as when a cold neutron star is heated by accretion of material from a companion. We focus on the temperature-density regime where plasma is in the liquid state and, therefore, the conductivity is dominated by the electron scattering off correlated nuclei. The dynamical screening of this interaction is implemented in terms of the polarization tensor computed in the hard-thermal-loop effective field theory of QED plasma. The correlations of the background ionic component are accounted for via a structure factor derived from Monte Carlo simulations of one-component plasma. With this input we solve the Boltzmann kinetic equation in relaxation time approximation taking into account the anisotropy of transport due to the magnetic field. The electrical conductivity tensor is studied numerically as a function of temperature and density for carbon and iron nuclei as well as density-dependent composition of zero-temperature dense matter in weak equilibrium with electrons. We also provide accurate fit formulas to our numerical results as well as supplemental tables which can be used in dissipative magneto-hydrodynamics simulations of warm compact stars.

DOI: [10.1103/PhysRevC.94.025805](https://doi.org/10.1103/PhysRevC.94.025805)**I. INTRODUCTION**

Electrical conductivity of crustal matter in neutron stars and interiors of white dwarfs plays a central role in the astrophysical description of these compact stars. The spectrum of problems where the conductivity of material is important includes magnetic field decay and internal heating, propagation of plasma waves, various instabilities, etc. Transport in highly compressed matter has been studied extensively in the cold regime, i.e., for temperatures $T \leq 1$ MeV (1.16×10^{10} K), which is relevant for neutron stars several minutes to hours past their formation in a supernova event, as well as for the interiors of white dwarfs. Initial studies of transport in dense matter appropriate for white dwarf stars go back to the work by Mestel and Hoyle [1] and Lee [2] in the 1950s, who computed the thermal conductivity of the electron-ion plasma in nonrelativistic electron regime, relevant for the radiative and thermal transport in white dwarfs. The electrical conductivity of ultracompressed matter, where electrons become relativistic (at zero temperature this corresponds to density 10^6 g cm⁻³) was computed by Abrikosov in 1963 [3] including the regime where matter is solid. These initial estimates were followed by a series of works in the 1960s and 1970s [4–12], among which the variational study of Flowers and Itoh [13] provides the most comprehensive account of transport in the solid and liquid regimes of crustal matter, as well as of the neutron drip regime, where free neutrons contribute to the thermal conductivity and shear viscosity of matter. An alternative formulation in terms of Coulomb logarithm and a detailed comparison of results of various authors was given in Ref. [14]. The regime where ions form a liquid was studied in Ref. [15], where it was shown that the screening of electron-ion interactions can

lead to substantial corrections in this case. These studies were further improved and extended in Refs. [16–25], which cover a broad range of densities and compositions appropriate for matter in white dwarfs and crusts of neutron stars in the case of strongly degenerate electrons and spherical nuclei. The special case of nonspherical nuclei (pasta phase) at the base of a neutron star crust, which may have very low electrical resistivity, is discussed in Ref. [26]. The implementation of the transport coefficients of dense matter in the dissipative magneto-hydrodynamics (MHD) equations was discussed and the associated transport coefficients in strong magnetic fields were computed for the crust of a cold neutron star in the presence of magnetic fields by a number of authors [16,20]. We confine our attention to nonquantizing fields in this work, i.e., fields below the critical field $B \simeq 10^{14}$ G above which the Landau quantization of electron trajectories becomes important [27].

The early computations of conductivity of cold neutron star matter described above were motivated by the studies of magnetic field decay in neutron star interiors. Recent resistive MHD simulations of magnetized neutron stars in general relativity [28–30], including binary magnetized neutron stars mergers and hypermassive neutron stars formed in the post-merger phase [31] require as an input the conductivity of warm (heated) crustal matter. In this regime the plasma forms a liquid state of correlated ions and ionized electrons at nonzero temperature and in nonzero magnetic field. Such matter is also expected in protoneutron stars newly formed in the aftermath of supernova explosion as well as in the crusts of neutron stars accreting material from a companion.

In this work we start addressing the necessary input for resistive MHD simulations of such matter, specifically its electrical conductivity. In this regime electrons are the most mobile charge carriers and the key mechanism of the electrical conduction is the electron scattering off the ions. There are important statistical corrections to the free-space

*arus@th.physik.uni-frankfurt.de

†sedrakian@th.physik.uni-frankfurt.de

scattering rate: following earlier calculations we incorporate structure factors of one-component plasma (we do not consider mixture here); in addition we include dynamical screening of exchanged photons which accounts for a frequency dependent scattering rate. The photon self-energy is computed within the hard-thermal-loop (HTL) effective field theory approach to polarization tensor.

The paper is organized as follows. Section II discusses the phase diagram of electron-ion plasma in the regimes of interest for neutron stars and white dwarfs. In Sec. III we derive the electrical conductivity tensor in magnetic field starting from the linearized Boltzmann equation for electrons. Section IV computes the matrix elements for electron-ion scattering including the screening of the interaction in the HTL approximation. We also discuss the input structure factor of ions (one-component plasma). In Sec. V we present the numerical results for the electrical conductivity in the density, temperature, and B -field regimes of interest. Our results are summarized in Sec. VI. Appendix A gives the details of the derivation of the relaxation time used in the main text and some numerical results. We describe the computations of polarization tensor in Appendix B.

We use the natural (Gaussian) units with $\hbar = c = k_B = k_e = 1$, $e = \sqrt{\alpha}$, $\alpha = 1/137$, and the metric signature $(1, -1, -1, -1)$.

II. PHYSICAL CONDITIONS

Matter in the interiors of white dwarfs and in the neutron star crusts is in a plasma state—the ions are fully ionized while free electrons are the most mobile carriers of charge. Electron density is related to the ion charge Z by charge conservation $n_e = Zn_i$, where n_i is the number density of nuclei. Electrons to a good accuracy form noninteracting gas which becomes degenerate below the Fermi temperature $T_F = \varepsilon_F - m$, where the Fermi energy $\varepsilon_F = (p_F^2 + m^2)^{1/2}$, the electron Fermi momentum is given by $p_F = (3\pi^2 n_e)^{1/3}$ and m is the electron mass. The state of ions with mass number A and charge Z is controlled by the value of the Coulomb plasma parameter

$$\Gamma = \frac{e^2 Z^2}{T a_i} \simeq 22.73 \frac{Z^2}{T_6} \left(\frac{\rho_6}{A} \right)^{1/3}, \quad (1)$$

where e is the elementary charge, T is the temperature, $a_i = (4\pi n_i/3)^{-1/3}$ is the radius of the spherical volume per ion, T_6 is the temperature in units 10^6 K, and ρ_6 is the density in units of 10^6 g cm $^{-3}$. If $\Gamma \ll 1$ or, equivalently $T \gg T_C \equiv Z^2 e^2/a_i$, ions form weakly coupled Boltzmann gas. In the regime $\Gamma \geq 1$ ions are strongly coupled and form a liquid for values of $\Gamma \leq \Gamma_m \simeq 160$ and a lattice for $\Gamma > \Gamma_m$. The melting temperature of the lattice associated with Γ_m is defined as $T_m = (Ze)^2/\Gamma_m a_i$. For temperatures below the ion plasma temperature

$$T_p = \left(\frac{4\pi Z^2 e^2 n_i}{M} \right)^{1/2}, \quad (2)$$

where M is the ion mass, the quantization of oscillations of the lattice becomes important. Figure 1 shows the temperature-

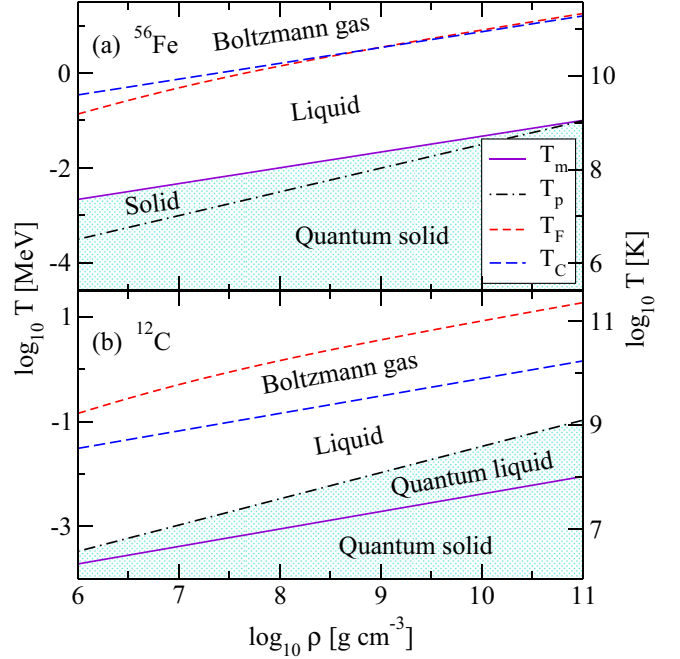


FIG. 1. The temperature-density phase diagram of dense plasma composed of iron ^{56}Fe (a) and carbon ^{12}C (b). The electron gas degeneracy sets in below the Fermi temperature T_F (short dashed lines). The ionic component solidifies below the melting temperature T_m (solid lines), while quantum effects become important below the plasma temperature (dash-dotted lines). For temperatures above T_C (long dashed lines) the ionic component forms a Boltzmann gas. Note that for ^{12}C the quantum effects become important in the portion of the phase diagram lying between the lines $T_p(\rho)$ and $T_m(\rho)$. The present study does not cover the shaded portion of the phase diagram.

density phase diagram of the crustal material in the cases where it is composed of iron ^{56}Fe (upper panel) and carbon ^{12}C (lower panel). The general structure of the phase diagram for ^{56}Fe shares many common features with the phase diagram of ^{12}C however there is one important difference: as the temperature is lowered the quantum effects become important for carbon prior to solidification, whereas iron solidifies close to the temperature where ionic quantum effects become important. Except for hydrogen and perhaps helium both of which may not solidify because of quantum zero point motions all heavier elements $Z > 2$ solidify at low enough temperature. Figure 2 shows the same phase diagram in the case of density-dependent crust composition adopted from Ref. [32] where nuclei are in weak equilibrium with electrons at zero temperature.

III. ELECTRICAL CONDUCTIVITY TENSOR

The kinetics of electrons is described by the Boltzmann equation for electron distribution function

$$\frac{\partial f}{\partial t} + \mathbf{v} \frac{\partial f}{\partial \mathbf{r}} - e(\mathbf{E} + [\mathbf{v} \times \mathbf{H}]) \frac{\partial f}{\partial \mathbf{p}} = I[f], \quad (3)$$

where \mathbf{E} and \mathbf{H} are the electric and magnetic fields, \mathbf{v} is the electron velocity, e is the unit charge, and $I[f]$ is the collision integral. In the relevant density and temperature regime

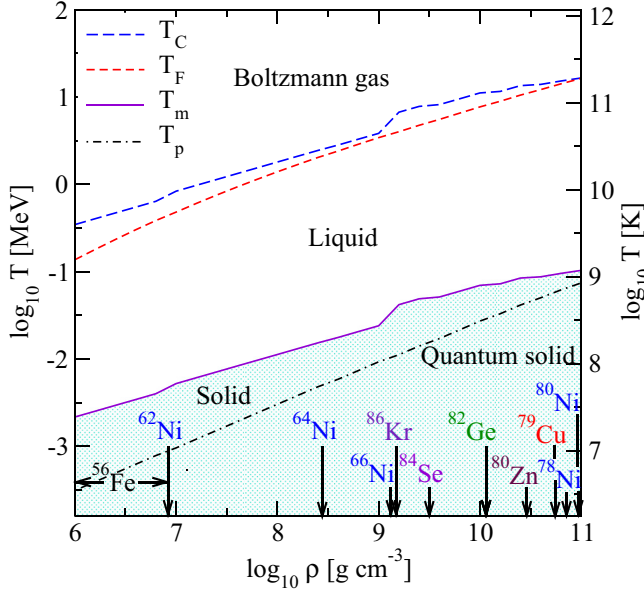


FIG. 2. The temperature-density phase diagram of dense stellar matter in the crust of a neutron star. Various phases are labeled in the figure. The vertical arrows show the density at which the indicated element first appears. The crust composition is taken from Ref. [32]. The shaded portion of the phase diagram indicates the regime which is not covered by our study.

electron-ion collisions are responsible for the conductivity of matter.¹ The collision integral has the form

$$I = -(2\pi)^4 \sum_{234} |\mathcal{M}_{12 \rightarrow 34}|^2 \delta^{(4)}(p + p_2 - p_3 - p_4) \times [f(1 - f_3)g_2 - f_3(1 - f)g_4], \quad (4)$$

where $f = f(p)$ and $f_3 = f(p_3)$ are the distribution functions of the incoming and outgoing electron, $g_{2,4} = g(p_{2,4})$ is the distribution function of the ion before and after collision; here and below we use the short-hand notation: $\sum_i = \int d\mathbf{p}_i / (2\pi)^3$. We will assume that ions form a classical ensemble in equilibrium, i.e., their distribution function $g(p)$ is given by the Maxwell-Boltzmann distribution

$$g(p) = n_i \left(\frac{2\pi}{MT} \right)^{3/2} e^{-\beta\varepsilon}, \quad (5)$$

where $\varepsilon = p^2/2M$, M is the ion mass, $\beta = T^{-1}$ is the inverse temperature, and n_i is the number density of ions. We are interested in perturbations that introduce small deviations from equilibrium, in which case the Boltzmann equation can be linearized. We thus consider small perturbation around the equilibrium Fermi-Dirac distribution function of electrons given by

$$f^0(\varepsilon) = \frac{1}{e^{\beta(\varepsilon - \mu)} + 1}, \quad (6)$$

¹Here we neglect the possible contribution from positrons, which can be sizable only in the very low density and high temperature matter.

where $\varepsilon = \sqrt{p^2 + m^2}$ and μ is the chemical potential and write

$$f = f^0 + \delta f, \quad \delta f = -\phi \frac{\partial f^0}{\partial \varepsilon}, \quad (7)$$

where $\delta f \ll f_0$ is a small perturbation. In the case of electrical conduction we can keep only the last term on the left-hand side of Eq. (3). We substitute for the electron distribution function (7) in Eq. (3) and take into account the identities

$$\frac{\partial f^0}{\partial \mathbf{p}} = \mathbf{v} \frac{\partial f^0}{\partial \varepsilon}, \quad \frac{\partial f^0}{\partial \varepsilon} = -\beta f^0(1 - f^0), \quad (8)$$

which follow directly from Eq. (6). To linear order in perturbation ϕ the Boltzmann equation reads

$$e\mathbf{v} \cdot \mathbf{E} \frac{\partial f^0}{\partial \varepsilon} - e[\mathbf{v} \times \mathbf{H}] \frac{\partial f^0}{\partial \varepsilon} \frac{\partial \phi}{\partial \mathbf{p}} = -I[f], \quad (9)$$

where the collision integral in the same approximation is given by

$$I[f] = -(2\pi)^4 \beta \sum_{234} |\mathcal{M}_{12 \rightarrow 34}|^2 \delta^{(4)}(p + p_2 - p_3 - p_4) \times f^0(1 - f_3^0)g_2(\phi - \phi_3). \quad (10)$$

The electric field appears in the drift term of linearized Boltzmann equation (9) at $O(1)$, whereas the term involving magnetic field at order $O(\phi)$, because $[\mathbf{v} \times \mathbf{H}](\partial f^0/\partial \mathbf{p}) \propto [\mathbf{v} \times \mathbf{H}]\mathbf{v} = 0$. We next specify the form of the function ϕ in the case of conduction as

$$\phi = \mathbf{p} \cdot \boldsymbol{\Xi}(\varepsilon), \quad (11)$$

which after substitution in Eqs. (9) and (10) gives

$$e\mathbf{v} \cdot [\mathbf{E} + (\boldsymbol{\Xi} \times \mathbf{H})] = -\boldsymbol{\Xi} \cdot \mathbf{p} \tau^{-1}(\varepsilon), \quad (12)$$

where the relaxation time is defined by

$$\tau^{-1}(\varepsilon) = (2\pi)^{-5} \int d\omega d\mathbf{q} \int d\mathbf{p}_2 |\mathcal{M}_{12 \rightarrow 34}|^2 \frac{\mathbf{q} \cdot \mathbf{p}}{p^2} \times \delta(\varepsilon - \varepsilon_3 - \omega) \delta(\varepsilon_2 - \varepsilon_4 + \omega) g_2 \frac{1 - f_3^0}{1 - f^0}. \quad (13)$$

In transforming the linearized collision integral we introduced a dummy integration over energy and momentum transfers, i.e., $\omega = \varepsilon - \varepsilon_3$ and $\mathbf{q} = \mathbf{p} - \mathbf{p}_3$. It remains to express the vector $\boldsymbol{\Xi}$ describing the perturbation in terms of physical fields. Its most general decomposition is given by

$$\boldsymbol{\Xi} = \alpha \mathbf{e} + \beta \mathbf{h} + \gamma [\mathbf{e} \times \mathbf{h}], \quad (14)$$

where $\mathbf{h} \equiv \mathbf{H}/H$ and $\mathbf{e} \equiv \mathbf{E}/E$ and the coefficients α , β , γ are functions of the electron energy. Substituting Eq. (14) in Eq. (12) one finds that $\alpha = -eE\tau/\varepsilon(1 + \omega_c^2\tau^2)$, $\beta/\alpha = (\omega_c\tau)^2(\mathbf{e} \cdot \mathbf{h})$ and $\gamma/\alpha = -\omega_c\tau$, where $\omega_c = eH\varepsilon^{-1}$ is the cyclotron frequency. As a result, the most general form of the perturbation is given by

$$\phi = -\frac{e\tau}{1 + (\omega_c\tau)^2} v_i [\delta_{ij} - \omega_c\tau \varepsilon_{ijk} h_k + (\omega_c\tau)^2 h_i h_j] E_j, \quad (15)$$

where the Latin indices label the components of Cartesian coordinates. The electrical current is defined in terms of perturbation ϕ as

$$j_i = 2 \int \frac{d\mathbf{p}}{(2\pi)^3} e v_i \phi \frac{\partial f^0}{\partial \varepsilon} \quad (16)$$

and, at the same time, it is related to the conductivity tensor σ_{ij} by

$$j_i = \sigma_{ij} E_j. \quad (17)$$

Substituting Eq. (15) in Eq. (16) and combining it with Eq. (17) we find for the conductivity tensor:

$$\sigma_{ij} = \delta_{ij} \sigma_0 - \varepsilon_{ijm} h_m \sigma_1 + h_i h_j \sigma_2, \quad (18)$$

where

$$\sigma_n = \frac{e^2 \beta}{3\pi^2} \int_m^\infty d\varepsilon \frac{p^3}{\varepsilon} \frac{\tau(\omega_c \tau)^n}{1 + (\omega_c \tau)^2} f^0 (1 - f^0), \quad n = 0, 1, 2. \quad (19)$$

The conductivity tensor has a simple form when the magnetic field is along the z direction:

$$\hat{\sigma} = \begin{pmatrix} \sigma_0 & -\sigma_1 & 0 \\ \sigma_1 & \sigma_0 & 0 \\ 0 & 0 & \sigma \end{pmatrix}. \quad (20)$$

Finally, note that in the absence of magnetic field $\mathbf{j} = \sigma \mathbf{E}$ with

$$\sigma = \frac{e^2 \beta}{3\pi^2} \int_m^\infty d\varepsilon \frac{p^3}{\varepsilon} \tau f^0 (1 - f^0) = \sigma_0 + \sigma_2. \quad (21)$$

IV. COLLISION INTEGRAL

We now turn to the evaluation of the collision integral, or equivalently the relaxation time, assuming that for temperatures and densities of interest relativistic electrons are scattered by correlated nuclei. In free space this process is described by the well-known Mott scattering by a Coulomb center. We use the standard QED methods to compute the transition probability, but include in addition the screening of the interaction by the medium in terms of polarization tensor.

A. Scattering matrix elements and relaxation time

The scattering amplitude for electron scattering off a nucleus characterized by its charge Z is given by (see Fig. 3 and Appendix B for details)

$$\mathcal{M}_{12 \rightarrow 34} = -\frac{J_0 J'_0}{q^2 + \Pi'_L} + \frac{\mathbf{J}_i \mathbf{J}'_i}{q^2 - \omega^2 + \Pi_T} = -\mathcal{M}_L + \mathcal{M}_T, \quad (22)$$

where

$$J^\mu = -e^* \bar{u}^{s_3}(p_3) \gamma^\mu u^s(p), \quad (23)$$

$$J'^\mu = Z e^* v'^\mu = Z e^* (1, \mathbf{p}'/M), \quad (24)$$

$e^* = \sqrt{4\pi} e$, and $\mathbf{J}_i, \mathbf{J}'_i$ are the components of the currents transversal to \mathbf{q} ($\mathbf{p}_1 \equiv \mathbf{p}$, $\mathbf{p}_2 \equiv \mathbf{p}'$). The screening of the

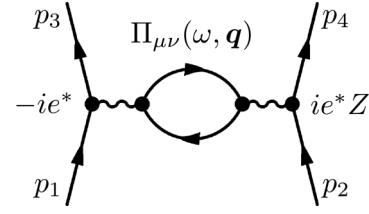


FIG. 3. Feynman diagram describing the scattering of electron of charge $e^* = \sqrt{4\pi} e$ off a nucleus of charge $e^* Z$ (left and right straight arrows, respectively) via exchange of photon (wavy line). The photon self-energy is given by the polarization tensor $\Pi_{\mu\nu}$ shown by the closed loop. Dots stand for QED vertices.

interaction is taken into account in terms of the longitudinal $\Pi_L(\omega, \mathbf{q})$ and transverse $\Pi_T(\omega, \mathbf{q})$ components of polarization tensor, with $\Pi'_L(\omega, \mathbf{q}) \equiv \Pi_L(\omega, \mathbf{q}) / (1 - \omega^2/q^2)$.

The form of the matrix element (22) includes thus the dynamical screening of the electron-ion interaction due to the exchange of transverse photons. Such separation has been employed previously in the treatment of transport of unpaired [33] and superconducting ultrarelativistic quark matter [34].

Standard QED diagrammatic rules can be applied to compute the transition probability from the diagram shown in Fig. 3. The square of the scattering matrix element can be written as

$$|\mathcal{M}_{12 \rightarrow 34}|^2 = |\mathcal{M}_L|^2 + |\mathcal{M}_T|^2 - 2\text{Re} \mathcal{M}_L \mathcal{M}_T^*, \quad (25)$$

where

$$|\mathcal{M}_L|^2 = \frac{J_0 J_0^* J'_0 J_0'^*}{|q^2 + \Pi'_L|^2}, \quad (26)$$

$$|\mathcal{M}_T|^2 = \frac{\mathbf{J}_i \mathbf{J}_i^* \mathbf{J}'_i \mathbf{J}'_i^*}{|q^2 - \omega^2 + \Pi_T|^2}, \quad (27)$$

$$\mathcal{M}_L \mathcal{M}_T^* = \frac{J_0 J_i^* J'_0 J_i'^*}{(q^2 + \Pi'_L)(q^2 - \omega^2 + \Pi_T^*)}, \quad (28)$$

i.e., the scattering probability is split into longitudinal, transverse, and interference contributions. The scattering probability per unit volume is obtained after averaging the scattering amplitude (25) over initial spins of electrons, summing over final spins, and multiplying with the structure factor of ions $S(q)$ and the square of nuclear form factor $F^2(q)$:

$$\sum_{s s_3} |\mathcal{M}_{12 \rightarrow 34}|^2 = \frac{Z^2 e^{*4}}{\varepsilon(\varepsilon - \omega)} S(q) F^2(q) \left\{ \frac{\varepsilon(2\varepsilon - \omega) - \mathbf{p} \cdot \mathbf{q}}{|q^2 + \Pi'_L|^2} + \frac{2(\mathbf{p}_i \cdot \mathbf{p}'_i)^2 + (p'_i)^2 (-\varepsilon\omega + \mathbf{p} \cdot \mathbf{q})}{M^2 |q^2 - \omega^2 + \Pi_T|^2} - \frac{2(2\varepsilon - \omega)(\mathbf{p}_i \cdot \mathbf{p}'_i)}{M \text{Re}[(q^2 + \Pi'_L)(q^2 - \omega^2 + \Pi_T^*)]} \right\}. \quad (29)$$

Substituting the transition probability in the expression for the relaxation time (13), carrying out the integrations (see

Appendix A for details) we finally obtain

$$\begin{aligned} \tau^{-1}(\varepsilon) &= \frac{\pi Z^2 e^4 n_i}{\varepsilon p^3} \int_{-\infty}^{\varepsilon-m} d\omega e^{-\omega/2T} \frac{f^0(\varepsilon-\omega)}{f^0(\varepsilon)} \\ &\times \int_{q_-}^{q_+} dq (q^2 - \omega^2 + 2\varepsilon\omega) S(q) F^2(q) \frac{1}{\sqrt{2\pi}\theta} \\ &\times e^{-\omega^2/2q^2\theta^2} e^{-q^2/8MT} \left\{ \frac{(2\varepsilon-\omega)^2 - q^2}{|q^2 + \Pi'_L|^2} \right. \\ &\left. + \theta^2 \frac{(q^2 - \omega^2)[(2\varepsilon-\omega)^2 + q^2] - 4m^2 q^2}{q^2 |q^2 - \omega^2 + \Pi_T|^2} \right\}, \end{aligned} \quad (30)$$

where $\theta \equiv \sqrt{T/M}$, $q_{\pm} = |\pm p + \sqrt{p^2 - (2\omega\varepsilon - \omega^2)}|$, and $\varepsilon = \sqrt{p^2 + m^2}$ for noninteracting electrons. The contributions of longitudinal and transverse photons in Eq. (30) separate (first and second terms in the braces). The dynamical screening effects contained in the transverse contribution are parametrically suppressed by the factor T/M at low temperatures and for heavy nuclei. This contribution is clearly important in the cases where electron-electron ($e-e$) scattering contributes to the collision integral. This is the case, for example, when ions form a solid lattice and, therefore, Umklapp $e-e$ processes are allowed, or in the case of thermal conduction and shear stresses when the $e-e$ collisions contribute to the dissipation.

Finally, to account for the finite size of the nuclei, we use the simple expression for the nuclear form factor [18]

$$F(q) = -3 \frac{qr_c \cos(qr_c) - \sin(qr_c)}{(qr_c)^3}, \quad (31)$$

where r_c is the charge radius of the nucleus given by $r_c = 1.15 A^{1/3}$ fm (see Appendix A for numerical results).

B. Recovering limiting cases

As shown in Appendix A when the ionic component of the plasma is considered at zero temperature and nuclear recoil can be neglected the relaxation time takes a simpler form

$$\tau^{-1}(\varepsilon) = \frac{\pi Z^2 e^4 n_i}{\varepsilon p^3} \int_0^{2p} dq q^3 S(q) F^2(q) \frac{4\varepsilon^2 - q^2}{|q^2 + \Pi'_L|^2}. \quad (32)$$

Consider now two limiting cases with respect to the temperature of the electronic component of the plasma, the degenerate limit, i.e., $T \ll T_F$ and the nondegenerate limit, i.e., $T \gg T_F$. In the zero-temperature limit Eqs. (19)–(21) simplify via the substitution $\partial f^0/\partial\varepsilon = -\beta f^0(1-f^0) \rightarrow -\delta(\varepsilon - \varepsilon_F)$, i.e.,

$$\sigma_n = \frac{e^2}{3\pi^2} \frac{p_F^3}{\varepsilon_F} \tau_F \frac{(\omega_{cF} \tau_F)^n}{1 + (\omega_{cF} \tau_F)^2} \quad (33)$$

and

$$\sigma = \frac{n_e e^2 \tau_F}{\varepsilon_F}, \quad \sigma_0 = \frac{\sigma}{1 + (\omega_{cF} \tau_F)^2}, \quad \sigma_1 = (\omega_{cF} \tau_F) \sigma_0, \quad (34)$$

where we used the expression for the electron Fermi momentum $p_F = (3\pi^2 n_e)^{1/3}$ and defined the relaxation time and cyclotron frequency at the Fermi energy, $\tau_F^{-1} \equiv \tau^{-1}(\varepsilon_F)$ and $\omega_{cF} = eB/\varepsilon_F$ (here and below we set $B = H$ which

corresponds to permeability of matter being unity). The first equation in Eq. (34) is the well-known Drude formula. From Eq. (32) we find in the low-temperature limit

$$\tau_F^{-1} = \frac{4Ze^4 \varepsilon_F}{3\pi} \int_0^{2p_F} dq q^3 \frac{S(q) F^2(q)}{|q^2 + \Pi'_L|^2} \left(1 - \frac{q^2}{4\varepsilon_F^2}\right), \quad (35)$$

where we used the charge neutrality condition $n_e = Zn_i$. Neglecting the screening ($\Pi'_L \rightarrow 0$) and the nuclear form factor [$F(q) \rightarrow 1$] we obtain from Eq. (35)

$$\tau_F^{-1} = \frac{4Ze^4 \varepsilon_F}{3\pi} \int_0^{2p_F} \frac{dq}{q} \left(1 - \frac{q^2}{4\varepsilon_F^2}\right) S(q), \quad (36)$$

which coincides with Eqs. (9) and (11) of Ref. [15].

In the limit of nondegenerate electrons $f^0 \ll 1$ and, therefore,

$$\begin{aligned} \sigma_n &\simeq \frac{e^2}{3\pi^2 T} \int_m^\infty p^2 dp \frac{p^2}{\varepsilon^2} \frac{\tau(\omega_c \tau)^n}{1 + (\omega_c \tau)^2} f^0 \\ &= \frac{n_e e^2}{3T} \left\langle v^2 \frac{\tau(\omega_c \tau)^n}{1 + (\omega_c \tau)^2} \right\rangle, \end{aligned} \quad (37)$$

where the quantities in the brackets are taken at some average energy $\bar{\varepsilon} \sim T$, which can be identified with the average thermal energy of a particle (electron) in the Boltzmann limit. We recall that the average of an energy-dependent quantity $F(\varepsilon)$ is defined as

$$\langle F(\varepsilon) \rangle = \frac{2}{n_e} \int \frac{d\mathbf{p}}{(2\pi)^3} F(\varepsilon) f^0(\varepsilon), \quad (38)$$

where a factor 2 arises from spin of electrons. In Eq. (37) we can further replace $v^2/3T \rightarrow 1/\bar{\varepsilon}$, consequently

$$\sigma \simeq \frac{n_e e^2 \bar{\tau}}{\bar{\varepsilon}}, \quad \sigma_0 \simeq \frac{\sigma}{1 + (\bar{\omega}_c \bar{\tau})^2}, \quad \sigma_1 \simeq \frac{\bar{\omega}_c \bar{\tau} \sigma}{1 + (\bar{\omega}_c \bar{\tau})^2}, \quad (39)$$

where $\bar{\omega}_c = eB/\bar{\varepsilon}$, $\bar{\tau} = \tau(\bar{\varepsilon})$. Thus, the formulas in both strongly degenerate and nondegenerate regimes have the same form, but different characteristic energy scale, which is ε_F in the degenerate regime and $\bar{\varepsilon} \simeq 3T$ in the nondegenerate, ultrarelativistic regime. In the case where $T \sim m$ we use $\bar{\varepsilon} = 3T/2 + \sqrt{(3T/2)^2 + m^2}$, which arises from the condition $\bar{v}^2 \bar{\varepsilon} = 3T$, where \bar{v} is the mean velocity.

C. Ion structure factor

For the numerical computations we need to specify the ion structure function $S(q)$. We assume that only one sort of ions exists at a given density, so that the structure factor of one-component plasma (OCP) can be used. These has been extensively computed using various numerical methods. We adopt the Monte Carlo results of Galam and Hansen [35] for Coulomb OCP provided in tabular form for $\Gamma \geq 2$ and set a two-dimension spline function in the space spanned by the magnitude of the momentum transfer q and the plasma parameter Γ . For small momentum transfers, $qa_i < 1$, we use the formulas (A1) and (A2) of Ref. [17].

In the low- Γ regime ($\Gamma \leq 2$), not covered by the Monte Carlo results, we use the analytical (leading order) expressions for Coulomb OCP by Tamashiro *et al.* [36] derived using density functional methods. The dependence of the resulting

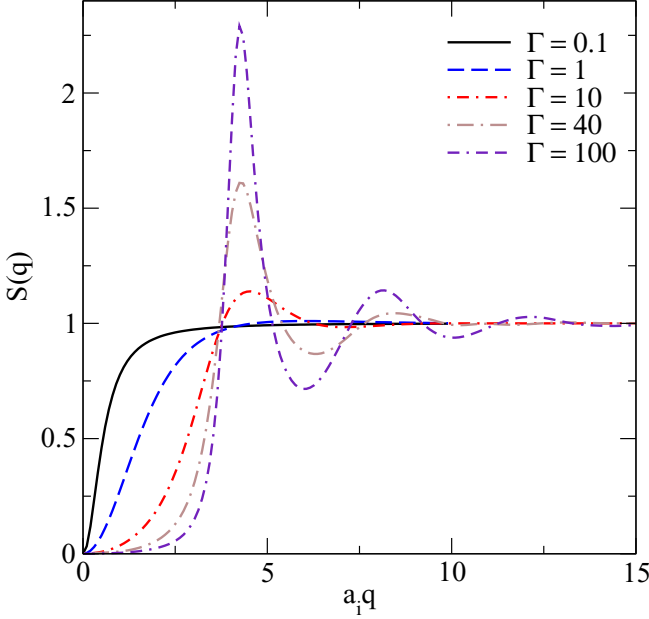


FIG. 4. Dependence of the structure factor of one-component plasma on the magnitude of momentum transfer q in units of inverse a_i . For $\Gamma \geq 2$ the structure factor is taken from Monte Carlo calculations of Galam and Hansen [35]. For $\Gamma < 2$ we obtain the structure factor from the analytical expressions provided by Tamashiro *et al.* [36].

structure factors on the dimensionless parameter $a_i q$, where a_i is the ion-sphere radius as defined after Eq. (1), is shown in Fig. 4 for various values of the plasma parameter Γ . Note that these correlation functions were derived for classical plasma, therefore the quantum aspects of motion of ^{12}C in the temperature regime $T_p \geq T \geq T_m$ are not accounted for. It is seen that the structure factor universally suppresses the contribution from small- q scattering. The suppression sets in for larger q at larger values of Γ . The large- q asymptotics is independent of Γ as $S(q) \rightarrow 1$. The major difference arises for intermediate values of q where the structure factor oscillates and the amplitude of oscillations increases with the value of Γ parameter. In addition to structure factor the scattering matrix is folded with the nuclear form factor, which accounts for the finite-size of individual nucleus. Its effect on the scattering matrix is small and is discussed in some detail in Appendix A.

D. Polarization tensor

The screening of longitudinal and transverse interactions is determined by the corresponding components of the photon polarization tensor. The expression (30) is exact with respect to the form of the polarization tensor. We will use an approximation to Eq. (30) derived within the HTL effective field theory of QED [37,38] in Appendix B; see also the related work on astrophysical relativistic, dense gases of Refs. [39–41]. Our computations, outlined in detail in Appendix B, are carried out at nonzero temperature and density and include the mass of leptons (electrons and positrons); formally, we require the four-momentum of the photon to be small compared with the four-momentum of the fermions in the loop. For the

longitudinal and transversal components of the polarization tensor we find

$$\Pi_L(q, \omega) = (1 - x^2) \int_0^\infty dp \mathcal{F}(\varepsilon) \left[1 - \frac{x}{2v} \log \frac{x+v}{x-v} \right], \quad (40)$$

$$\Pi_T(q, \omega) = \frac{1}{2} \int_0^\infty dp \mathcal{F}(\varepsilon) \left[x^2 + (v^2 - x^2) \frac{x}{2v} \log \frac{x+v}{x-v} \right], \quad (41)$$

where $x = \omega/q$ and $v = \partial\varepsilon/\partial p = p/\varepsilon$ is the particle velocity and

$$\mathcal{F}(\varepsilon) \equiv -\frac{4e^2}{\pi} p^2 \left[\frac{\partial f^+(\varepsilon)}{\partial \varepsilon} + \frac{\partial f^-(\varepsilon)}{\partial \varepsilon} \right]. \quad (42)$$

In the degenerate or ultrarelativistic limits the velocity has a constant value \bar{v} and Eqs. (40) and (41) can be written as

$$\Pi_L = q_D^2 (1 - x^2) \left[1 - \frac{x}{2\bar{v}} \log \frac{x+\bar{v}}{x-\bar{v}} \right], \quad (43)$$

$$\Pi_T = \frac{1}{2} q_D^2 \left[x^2 + (\bar{v}^2 - x^2) \frac{x}{2\bar{v}} \log \frac{x+\bar{v}}{x-\bar{v}} \right], \quad (44)$$

where $\bar{v} = v_F$ in the degenerate and $\bar{v} = 1$ in the ultrarelativistic limits, respectively, and the Debye wave number q_D is given by radial part of the phase-space integral

$$q_D^2 = \int_0^\infty dp \mathcal{F}(\varepsilon). \quad (45)$$

Dropping the contribution of antiparticles we find in the limiting cases of highly degenerate and nondegenerate matter

$$q_D^2 \simeq 4e^2 \begin{cases} p_F \varepsilon_F / \pi, & T \ll T_F, \\ \pi n_e / T, & T \gg T_F, \end{cases} \quad (46)$$

where in the last line we introduced the electron number density ($f^0 \equiv f^+$)

$$n_e = 2 \int \frac{d\mathbf{p}}{(2\pi)^3} f^0(\varepsilon). \quad (47)$$

Equations (43) and (44) coincide with Eqs. (8) and (9) of Ref. [40], if we take into account the first line of Eq. (46) and substitute $e^2 \rightarrow e^2/4\pi$ in our equations. Note that Eqs. (43) and (44) can be also applied in the general case, if \bar{v} is defined as the characteristic velocity of electrons.

At temperatures of interest it is more economical to use low $x \ll 1$ expansions for the polarization tensor (see Appendix A); we keep the next-to-leading in x terms and find

$$\Pi'_L(q, \omega) = q_D^2 \chi_l, \quad \Pi_T(q, \omega) = q_D^2 \chi_t, \quad (48)$$

where the susceptibilities to order $O(x^2)$ are given by

$$\text{Re}\chi_l(q, \omega) = 1 - \frac{x^2}{\bar{v}^2}, \quad \text{Im}\chi_l(q, \omega) = -\frac{\pi x}{2\bar{v}}, \quad (49)$$

$$\text{Re}\chi_t(q, \omega) = x^2, \quad \text{Im}\chi_t(q, \omega) = \frac{\pi}{4} x \bar{v}. \quad (50)$$

Because the terms containing \bar{v} are small as well as electrons are ultrarelativistic in the most of the regime of interest we approximate $\bar{v} = 1$ in our numerical calculations.

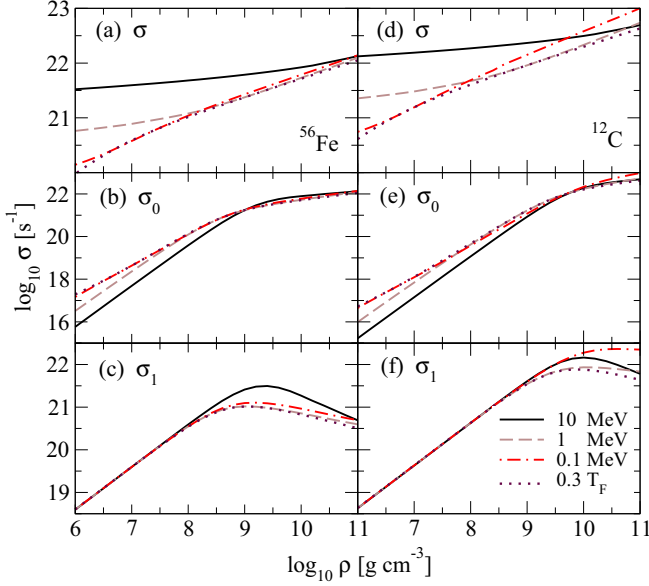


FIG. 5. Dependence of three components of the electrical conductivity tensor on density for various values of temperature indicated in the plot and $B_{12} = 1$ ($B_{12} \equiv B/10^{12}$ G). (a)–(c) show the conductivities for ^{56}Fe , (d)–(f) the same for ^{12}C .

V. RESULTS

Numerically the electrical conductivity is evaluated using the relaxation time Eq. (30) in the most general case with the ion structure factor given in Fig. 4 and polarization tensor given by Eqs. (48)–(50). With this relaxation time we evaluate the components of the conductivity tensor using Eq. (19). We recall that for large magnetic fields the tensor structure of the conductivity is important, while in the limit of negligible fields only the single quantity $\sigma = \sigma_0 + \sigma_2$ is relevant, see Eq. (21).

A. Low-field limit

We start our analysis of the numerical results with the density, temperature, and composition dependence of conductivity σ in low magnetic fields given by Eq. (21). We relegate to the next section the discussion of the σ_0 and σ_1 components, which is straightforward after we clarified the basic features of σ . We will also first study the cases of ^{56}Fe and ^{12}C and later on consider density-dependent composition of crustal matter in Sec. V C. The upper panels of Fig. 5 show σ as a function of density for various temperatures and magnetic field $B_{12} = 1$; here and below we use the units $B_{12} = B/10^{12}$ G to characterize the magnetic field. The temperature values range from the nondegenerate regime ($T = 10$ MeV) to the degenerate regime ($T = 0.1$ MeV) where the case $T = 1$ MeV is representative for transition from nondegenerate to degenerate regime, which occurs at around $\log_{10}\rho \simeq 8$ g cm $^{-3}$ for both ^{56}Fe and ^{12}C nuclei (see Fig. 1). In each case σ shows a power-law dependence on density $\sigma \propto \rho^\alpha$; in the degenerate regime $\alpha \simeq 0.4$ for ^{56}Fe and $\alpha \simeq 0.45$ for ^{12}C . In the nondegenerate regime the increase is less steep with $\alpha \simeq 0.1$ for both ^{56}Fe and ^{12}C .

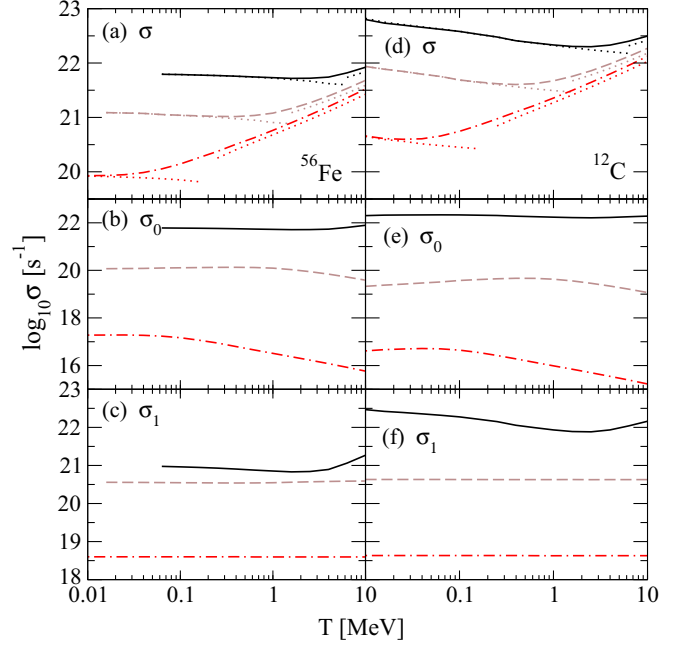


FIG. 6. The temperature dependence of three components of the electrical conductivity tensor for $B_{12} = 1$ and three values of density— $\log_{10}\rho = 10$ (solid lines), $\log_{10}\rho = 8$ (dashed lines), $\log_{10}\rho = 6$ (dash-dotted lines) in units [g cm $^{-3}$]. (a)–(c) show the conductivities for ^{56}Fe , (d)–(f) the same for ^{12}C . The dots represent the results obtained with Eqs. (34) and (39).

This behavior can be traced back to the different density and temperature dependence of the relaxation time in these regimes. The conductivity depends in both regimes on the ratio $\tau(\varepsilon)/\varepsilon$ and is proportional to n_e , see Eqs. (34) and (39). For any fixed temperature and density, the ratio $\tau(\varepsilon)/\varepsilon$ scales approximately as ε . In the degenerate regime ε is the Fermi energy, therefore, $\varepsilon \propto \rho^{1/3}$, while in the nondegenerate regime $\varepsilon \propto T$ independent of density. Apart from these differences, $\tau^{-1} \propto n_i$ which guarantees that the relaxation time decreases with density in both cases. These factors combined lead to slower increase of conductivity in the nondegenerate regime as compared to the degenerate one. Note that $\omega_c\tau$ scales as τ/ε in both cases (see Appendix A for further details).

The main difference between the values of σ for different nuclei characterized by their mass number A and charge Z is due to the scaling $\tau^{-1} \sim Z^2 n_i \sim Z^2/A \sim Z$; for not very heavy elements $Z/A \simeq 0.5$, see Eq. (30). Therefore, we find for the ratio of conductivities of ^{12}C to ^{56}Fe : $\sigma_{\text{C}}/\sigma_{\text{Fe}} \simeq \tau_{\text{C}}/\tau_{\text{Fe}} \simeq Z_{\text{Fe}}/Z_{\text{C}} \simeq 4.3$, which is consistent with the results shown in Fig. 5.

Let us turn to the temperature dependence of the conductivity. The most prominent effect seen in the temperature dependence of σ , shown in Fig. 6, is the existence of a minimum as a function of temperature. The dotted lines in the low-temperature regime correspond to the formula (34) and extend to the point where $T \simeq T_F$. We see that the Drude formula works very well for $T \leq 0.1T_F$ and we find a good agreement between our conductivities and those in Refs. [15,24]. The dotted lines in the high-temperature

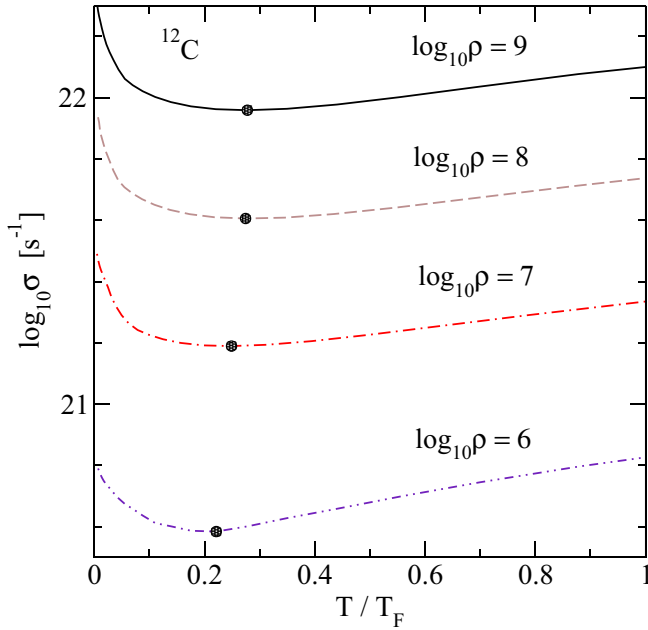


FIG. 7. Dependence of conductivity on the scaled temperature for various densities. The minimum of the conductivity occurs roughly at $T \simeq T^*$.

regime correspond to the formula (39). As we see from the plots, Eq. (39) gives the correct qualitative behavior of the electrical conductivity at high temperatures, but quantitatively underestimates it by about 20%. The minimum in σ arises at about the transition from the degenerate to nondegenerate regime and is identified empirically with $T^* \equiv 0.3T_F$. (This approximately corresponds to the requirement that the Fermi energy becomes equal to the thermal energy of a nondegenerate gas). We show in Fig. 7 the dependence of σ on appropriately scaled temperature for a number of densities for ^{12}C (the results are similar also in the case of ^{56}Fe). We also show the density dependence of the conductivity at the minimum in Fig. 5. The conductivity decreases with temperature at low temperatures, when the electrons are degenerate. This decrease arises solely from the temperature dependence of the correlation function $S(q)$. In the case $S(q) = 1$ the relaxation time is nearly temperature independent, whereas in full calculation it decreases with temperature, as expected (see Appendix A for numerical illustrations). Indeed, as seen from Fig. 4, with increasing temperature and, consequently, decreasing Γ small momentum transfer scattering becomes more important which increases the effective cross section.

In the nondegenerate regime the temperature dependence of τ changes, because $\bar{\tau} \propto \bar{\epsilon}^2$, therefore conductivity $\sigma \propto \bar{\tau}/\bar{\epsilon} \propto T$, as suggested in Ref. [13] (the exact calculations give $\sigma \propto T^\beta$ with $\beta \simeq 0.7-0.8$).

In the degenerate regime the temperature dependence of σ (or τ) is stronger for lighter elements, because for the given density and temperature the parameter Γ is smaller for lighter elements ($\Gamma \sim Z^2/A^{1/3}$, $\Gamma_{\text{Fe}}/\Gamma_{\text{C}} \simeq 11$), and the $S(q; \Gamma)$ varies faster for small values of Γ , see Fig. 4.

B. Strong fields

For strong magnetic fields the tensor structure of the conductivity becomes important and we need to discuss the remaining components of this tensor given by Eqs. (34) and (39). These components depend strongly on the value of “anisotropy parameter” $\omega_c \tau$. Assuming density independent values of the magnetic fields, we find that the parameter $\omega_c \tau$ decreases as a function of density because of the decrease of relaxation time in any regime, see Fig. 14 of Appendix A. Note that in the degenerate case ω_c decreases as well because of its inverse dependence on the energy of electrons. It is seen that at high densities $\omega_c \tau \ll 1$ (isotropic region) and $\sigma_0 \simeq \sigma$. At low densities $\omega_c \tau \gg 1$ (strongly anisotropic region) and we have

$$\sigma_0 \simeq \frac{\sigma}{(\omega_c \tau)^2} \simeq \left(\frac{n_e e}{B} \right)^2 \sigma^{-1} \ll \sigma. \quad (51)$$

As $\omega_c \tau$ decreases with the density, σ_0 increases with density much faster than σ : $\sigma_0 \propto \rho^\beta$, $\beta \simeq 1.5$ in the degenerate and $\beta \simeq 1.9$ in the nondegenerate regime. At low densities σ_0 is smaller than σ by several orders of magnitude, the exact value being dependent on magnetic field.

We see from Eq. (51) that for a given density $\sigma_0 \sim \sigma^{-1}$, therefore σ_0 shows a reversed temperature dependence at low densities. It increases in the degenerate regime, decreases in the nondegenerate regime, see Fig. 6, and has a maximum at temperature T^* . The reversed behavior applies also to the Z -dependence, i.e., $\sigma_0 \sim \tau^{-1} \sim Z$, therefore σ_0 is smaller for lighter elements. The curves corresponding to different temperatures in Fig. 5 intersect when $\omega_c \tau \simeq 1$ at high density ($\rho \simeq 10^9 \text{ g cm}^{-3}$) as a consequence of transition from anisotropic to isotropic conduction (see also Fig. 14). In addition, there are also intersections related to the transition from degenerate (high-density) to nondegenerate (low-density) regime, as already discussed in the case of σ .

For σ_1 component we have

$$\sigma_1 \simeq \sigma \omega_c \tau \simeq \frac{B}{n_e e} \sigma^2, \quad \omega_c \tau \ll 1, \quad (52)$$

$$\sigma_1 \simeq \frac{\sigma}{\omega_c \tau} \simeq \frac{n_e e}{B}, \quad \omega_c \tau \gg 1. \quad (53)$$

At low densities ($\omega_c \tau \gg 1$) σ_1 is proportional to the density and depends neither on temperature, nor on the type of nuclei, see Eq. (53). At high densities σ_1 becomes a decreasing function of density because of the additional factor $\omega_c \tau$ in Eq. (52), the decrease being faster at higher temperatures, see Fig. 5. We find the scaling $\sigma_1 \propto \rho^{-\gamma}$, $\gamma \simeq 0.2$ in the degenerate and $\gamma \simeq 0.7$ in the nondegenerate regime. As a function of density σ_1 has a maximum at $\omega_c \tau \simeq 1$, where $\sigma_0 \simeq \sigma_1 \simeq \sigma/2$. In isotropic region σ_1 depends on the temperature through the scaling $\sigma_1 \sim \sigma^2$ and has a minimum at T^* . Because $\sigma_1 \sim Z^2$, it is larger for ^{12}C as compared to ^{56}Fe by more than an order of magnitude. As τ is larger for light elements, the anisotropic region for these elements is larger, and the maximum of σ_1 versus density is shifted to higher densities and its value increases, as can be seen from Figs. 5 and 8. Note that in both isotropic and strongly anisotropic cases $\sigma_1 \ll \sigma$. Figures 8 and 9 show the dependence of σ_0 and σ_1 on the magnetic

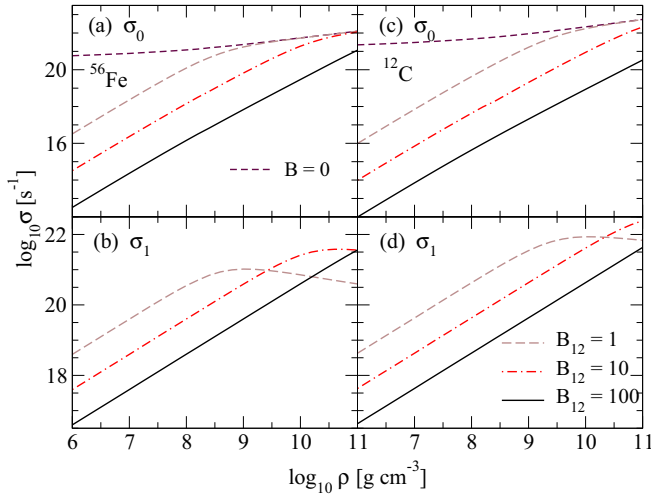


FIG. 8. Dependence of σ_0 [(a) and (c)] and σ_1 [(b) and (d)] components of the conductivity tensor on density for various values of the B -field. (a) and (b) show these components for ^{56}Fe , (c) and (d) the same for ^{12}C . The temperature is fixed at $T = 1$ MeV.

field. As $\omega_c \propto B$, the density region where the conductivity is anisotropic becomes larger with the increase of magnetic field, and the maximum of σ_1 as a function of density is shifted to higher densities (see Fig. 8).

For low magnetic fields $\sigma_0 \simeq \sigma$ (Fig. 9). With increasing magnetic field σ_0 decreases and for $\omega_c \tau \gg 1$ we find that $\sigma_0 \propto B^{-2}$, see Eq. (51). For $\omega_c \tau \ll 1$ and $\omega_c \tau \gg 1$ cases we have $\sigma_1 \propto B$ and $\sigma_1 \sim B^{-1}$, respectively, see Eqs. (52) and (53), therefore σ_1 should have a maximum as a function of magnetic field. As seen from Fig. 9, the maximum of σ_1 occurs where σ_0 begins to drop ($\omega_c \tau \simeq 1$). This maximum shifts to lower magnetic fields with the decrease of density and charge Z . For

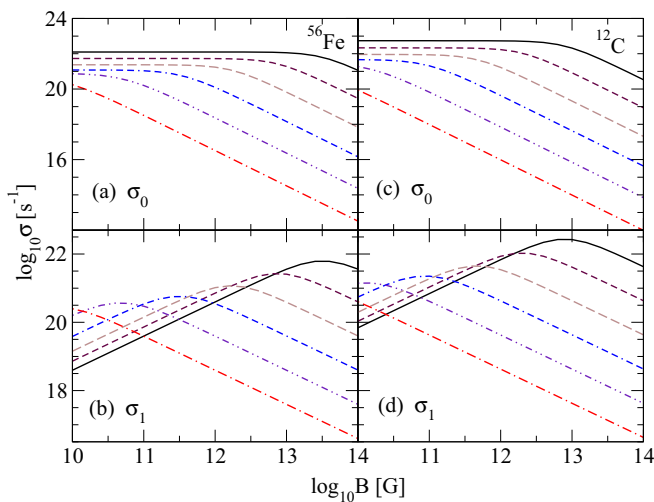


FIG. 9. Dependence of σ_0 (upper panels) and σ_1 (lower panels) components of the conductivity tensor on the magnetic field for ^{56}Fe (left panels) and ^{12}C (right panels) at six values of density— $\log_{10} \rho = 11$, $\log_{10} \rho = 10$, $\log_{10} \rho = 9$, $\log_{10} \rho = 8$, $\log_{10} \rho = 7$, $\log_{10} \rho = 6$ (from top to bottom). The temperature is fixed at $T = 1$ MeV.

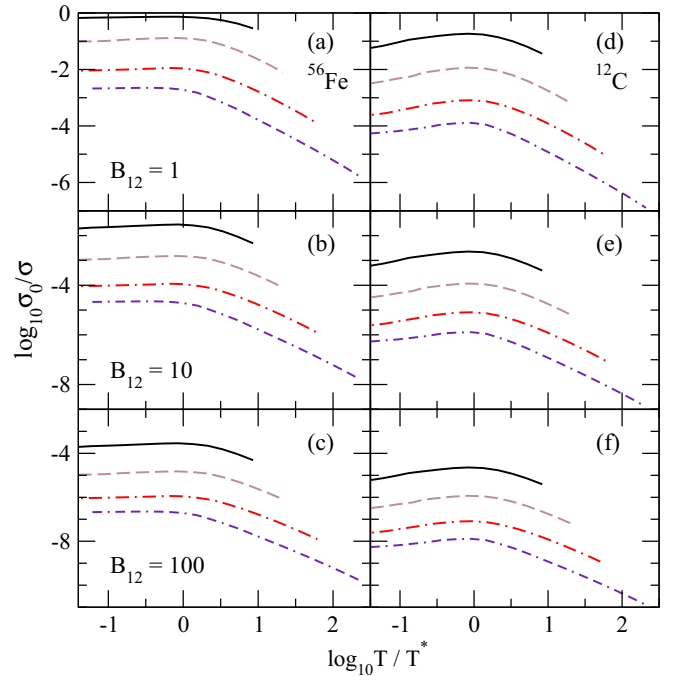


FIG. 10. The ratio σ_0/σ as a function of scaled temperature T/T^* at various densities $\log_{10} \rho = 9$ (solid lines), $\log_{10} \rho = 8$ (dashed lines), $\log_{10} \rho = 7$ (dash-dotted lines), and $\log_{10} \rho = 6$ (double-dash-dotted lines) and for three values of magnetic field $B_{12} = 1$ [(a) and (d)], $B_{12} = 10$ [(b) and (e)], and $B_{12} = 100$ [(c) and (f)]. (a)–(c) show the ratio for ^{56}Fe , (d)–(f) the same for ^{12}C .

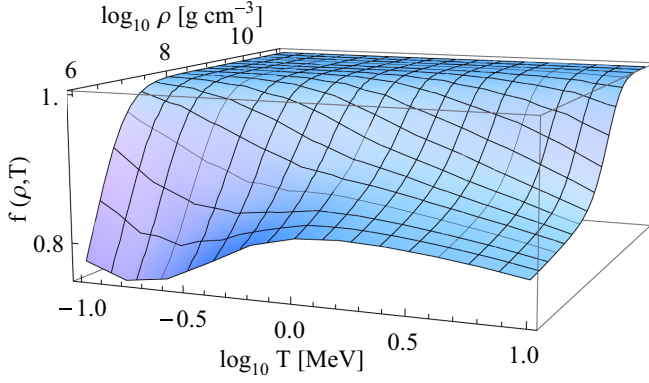
$B = 10^{12}$ G the crust is anisotropic at densities $\rho < 10^9$ g cm $^{-3}$ for ^{56}Fe and $\rho < 10^{10}$ g cm $^{-3}$ for ^{12}C . For magnetic fields $B \geq 10^{13}$ G the outer crust is almost completely anisotropic.

We now turn to the study of combined effects of temperature and magnetic field, i.e., how the anisotropy induced by the magnetic field is affected by the temperature. To characterize the anisotropy we consider the ratio σ_0/σ , which is shown in Fig. 10 as a function of dimensionless ratio T/T^* for various densities and magnetic fields. We see that all curves have a maximum at $T = T^*$ independent of density, magnetic field, and type of nuclei. At this maximum the anisotropy is smallest. As $\sigma_0/\sigma \propto \sigma^{-2}$, see Eq. (51), it increases with the temperature in the degenerate regime. In the nondegenerate regime σ increases with temperature, therefore σ_0/σ decreases approximately as $T^{-3/2}$. At very high temperatures the crust becomes strongly anisotropic.

From Eqs. (34) and (39) we can obtain a simple relation between the three components of the conductivity tensor

$$f(\rho, T) \equiv \frac{\sigma_0}{\sigma} \left[1 + \left(\frac{\sigma_1}{\sigma_0} \right)^2 \right] = 1. \quad (54)$$

At temperatures close to the Fermi temperature Eqs. (34) and (39) break down, however, according to Fig. 11 the relation (54) is satisfied quite well in the whole crust. While Fig. 11 shows the case for ^{56}Fe , we have verified that similar results hold for ^{12}C and composition dependent crust and are weakly dependent on the magnitude of the magnetic field $1 \leq B_{12} \leq 100$.


 FIG. 11. The function $f(\rho, T)$ for ^{56}Fe at magnetic field $B_{12} = 1$.

C. Density-dependent composition

We now turn to the case where the composition of matter depends on the density. We will assume that the composition does not depend strongly on the temperature in the range of temperatures studied here ($T \leq 10$ MeV) and will proceed with composition derived for $T = 0$. The conservation of baryon number, electric charge and the condition of β -equilibrium uniquely determines the energetically most preferable state of matter for any given model of nuclear forces in the density range of interest $10^6 \leq \rho \leq \rho_{\text{drip}}$, where $\rho_{\text{drip}} \simeq 4 \times 10^{11} \text{ g cm}^{-3}$ is the neutron drip density.

The laboratory information on nuclear masses can be used as an input to eliminate the uncertainties related to the nuclear Hamiltonian [42], therefore various studies of the composition of the crusts predict nearly identical sequences of nuclei as a function of density.

In our calculations we adopted the nuclear sequence shown in Fig. 2 taken from Ref. [32], which predicts matter composed of iron below the density $\log_{10}\rho \leq 7$ which is followed by a sequence of nuclei with charges in the range $28 \leq Z \leq 36$. This composition can be compared to the initial studies of nuclear sequences below neutron drip density [43,44] (displayed in Table 2.1 of Ref. [44]) and a more recent study based on improved data and theory [45]. These deviate from the composition adopted here only marginally.

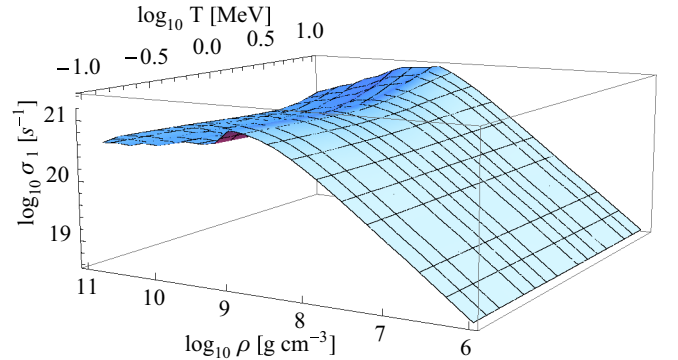
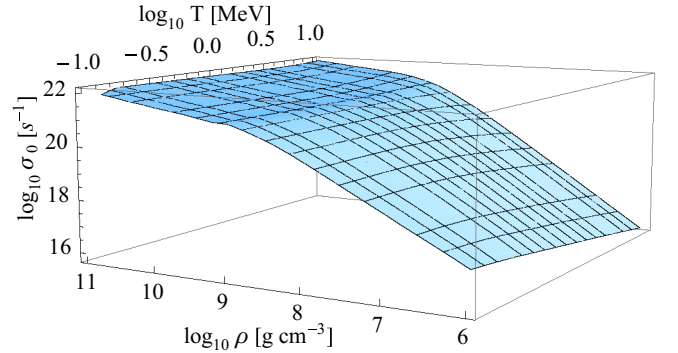
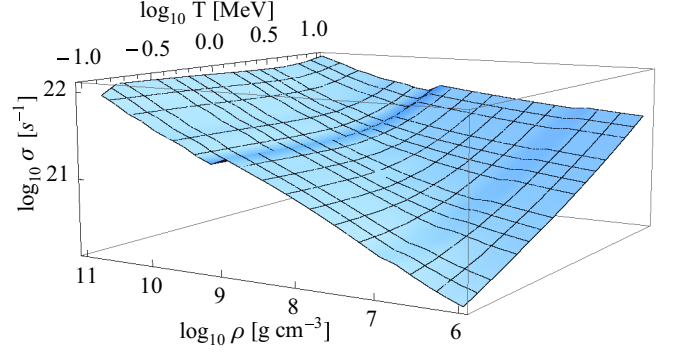
To assess the differences that arise from the replacement of, for example, iron nuclei studied above by density-dependent composition recall that for nuclei with mass number A and charge Z the relaxation time scales as $\tau^{-1} \propto Z^2 n_i \propto Z^2/A$. Because $\tau \propto \varepsilon^2$, in the degenerate regime there will be additional density dependence in the conductivity arising from the factor $\tau/\varepsilon \propto n_e^{1/3}$. For the conductivity in the degenerate regime we find the scaling

$$\sigma \propto \frac{n_e \tau_F}{\varepsilon_F} \propto \left(\frac{Z}{A}\right)^{1/3} Z^{-1}. \quad (55)$$

In the nondegenerate regime

$$\sigma \propto \frac{n_e \bar{\tau}}{\bar{\varepsilon}} \propto Z^{-1}. \quad (56)$$

To give a few numerical examples, we quote the ratio \mathcal{R} of conductivities of elements present in density-dependent


 FIG. 12. Dependence of three components of the electrical conductivity tensor on density and temperature for $B_{12} = 1$ and composition taken from Ref. [32].

matter composition to that of iron: $\mathcal{R}[^{62}\text{Ni}] = 0.92$, $\mathcal{R}[^{64}\text{Ni}] = 0.91$, $\mathcal{R}[^{86}\text{Kr}] = 0.70$, $\mathcal{R}[^{84}\text{Se}] = 0.73$, $\mathcal{R}[^{82}\text{Ge}] = 0.77$, $\mathcal{R}[^{80}\text{Zn}] = 0.81$, $\mathcal{R}[^{80}\text{Ni}] = 0.85$ in the degenerate regime and $\mathcal{R}[^{62}\text{Ni}] = \mathcal{R}[^{64}\text{Ni}] = 0.93$, $\mathcal{R}[^{86}\text{Kr}] = 0.72$, $\mathcal{R}[^{84}\text{Se}] = 0.76$, $\mathcal{R}[^{82}\text{Ge}] = 0.81$, $\mathcal{R}[^{80}\text{Zn}] = 0.87$, $\mathcal{R}[^{80}\text{Ni}] = 0.93$ in the nondegenerate regime. The discrepancies between these estimates based on the scalings (55) and (56) and our numerical results are smaller than 5% and arise from the additional dependence of the relaxation time on Z and A via the structure factor and the Debye momentum. We conclude that the composition dependent results differ from those found for iron by a factor ≤ 1.4 .

The three components of the conductivity tensor in the case of density-dependent composition are shown in Fig. 12 and,

according to the arguments above, show all the basic features already discussed in the case of ^{56}Fe .

D. Fit formulas for the electrical conductivity tensor

We have performed fits to the first component of the conductivity tensor using the formula

$$\sigma^{\text{fit}} = CZ^{-1}T_F^a \left(\frac{T}{T_F}\right)^{-b} \left(\frac{T}{T_F} + d\right)^{b+c}, \quad (57)$$

where $C = 1.5 \times 10^{22} \text{ s}^{-1}$, T , T_F are in MeV units and σ^{fit} is in s^{-1} . The density dependence of σ^{fit} arises from its dependence on the Fermi temperature, which in general has the form $T_F = 0.511[\sqrt{1 + (Z\rho_6/A)^{2/3}} - 1]$. For ultrarelativistic electrons this simplifies to $T_F = 0.511(Z\rho_6/A)^{1/3} \simeq 0.4\rho_6^{1/3}$, where to obtain the second relation we assumed for simplicity $Z/A \simeq 0.5$. Substituting this into Eq. (57) we obtain a fit formula with explicit dependence on density

$$\sigma^{\text{fit}} = C'Z^{-1}\rho_6^{(a+b)/3}T^{-b}(T\rho_6^{-1/3} + d')^{b+c}, \quad (58)$$

where $C' = 0.4^{a-c}C$ and $d' = 0.4d$.

The fit parameters a, b, c, d depend on the ionic structure of the material. The maximal relative error of the fit formula is defined as $\gamma = 100|\sigma^{\text{fit}} - \sigma|/\sigma$. The values of fitting coefficients in various cases are as follows:

- (i) Matter composed of ^{12}C , $\gamma \simeq 8\%$,

$$a = 0.919, \quad b = 0.372, \quad c = 0.813, \quad d = 0.491. \quad (59)$$

- (ii) Matter composed of ^{56}Fe , $\gamma \simeq 10\%$,

$$a = 0.931, \quad b = 0.149, \quad c = 0.850, \quad d = 0.832. \quad (60)$$

- (iii) β -equilibrium composition, $\gamma \simeq 10\%$,

$$a = 0.935, \quad b = 0.126, \quad c = 0.852, \quad d = 0.863. \quad (61)$$

The form of Eq. (57) provides the correct temperature and density dependence of the conductivity in the limiting cases of strongly degenerate and nondegenerate electrons. For the first case $T \ll T_F$ and $\sigma \propto T_F^{a+b}T^{-b}$. In the nondegenerate limit $T \gg T_F$ and $\sigma \propto T_F^{a-c}T^c$. As to the explicit density dependence in these limits, one finds that $\sigma \propto \rho^{(a+b)/3}T^{-b}$ when $T \ll T_F$ and $\sigma \propto \rho^{(a-c)/3}T^c$ when $T \gg T_F$ assuming ultrarelativistic limit. Averaging the fit parameters we finally quote the rough scaling of the conductivity in the limiting cases: $\sigma \propto \rho^{1/3}T^{-1/3}$ for ^{12}C and $\sigma \propto \rho^{1/3}T^{-1/7}$ in the other cases in the degenerate regime and $\sigma \propto \rho^{1/30}T^{4/5}$ in the nondegenerate regime.

For the other two components of the conductivity tensor the following formulas can be used

$$\sigma_0^{\text{fit}} = \frac{\sigma'}{1 + \delta^2\sigma'^2}, \quad \sigma' = \sigma^{\text{fit}} \left(\frac{T_F}{\varepsilon_F}\right)^g, \quad (62)$$

$$\sigma_1^{\text{fit}} = \frac{\delta\sigma''^2}{1 + \delta^2\sigma''^2}, \quad \sigma'' = \sigma^{\text{fit}} \left(1 + \frac{T}{T_F}\right)^h, \quad (63)$$

where $\delta = B(n_e ec)^{-1}$ in cgs units with c being the speed of light, $g = 0.16$, and

$$h[^{12}\text{C}] = 0.075, \quad h[^{56}\text{Fe}] = 0.025, \quad h[\text{comp.}] = 0.045,$$

where the last number refers to β -equilibrium composition.

The relative error of Eq. (62) is $\gamma \simeq 11\%$ for ^{12}C and $\gamma \simeq 13\%$ for ^{56}Fe and β -equilibrium composition. The relative error of Eq. (63) is $\gamma \simeq 12\%$ for ^{12}C and $\gamma \simeq 15\%$ for ^{56}Fe and β -equilibrium composition at temperatures $T > 0.15 \text{ MeV}$.

VI. CONCLUSIONS

Motivated by recent advances in numerical simulations of astrophysical phenomena such as mergers of neutron star binaries within the resistive MHD framework we have computed here the conductivity of warm matter ($10^9 \leq T \leq 10^{11} \text{ K}$) at densities corresponding to the outer crusts of neutron stars and interiors of white dwarfs. Our results apply to arbitrary temperatures above the solidification temperature of matter and cover the transition from the degenerate to the non-degenerate regimes. In this liquid plasma regime the conductivity is dominated by the electrons which scatter off the correlated nuclei via screened electromagnetic force. The correlations in the plasma in the liquid state are included in terms of ion structure function extracted from the data on Monte Carlo simulations of one-component plasma (OCP). A key feature of our computation is the inclusion of the dynamical screening of photon exchange and inelastic processes, which we show to be small in the temperature-density regime considered. The use of OCP structure factor implies that our results should be applied with caution in the case where matter is composed of mixture of nuclei, in which case the interspecies correlations are not accounted for. We have implemented the HTL QED polarization susceptibilities in the low-frequency limit combined with non-zero-temperature screening Debye length, which should be a good approximation where the inelastic processes are suppressed by the large mass of nuclei. A further simplifying approximation that went into our formalism, which is well justified by the MHD regime of astrophysical studies, is the assumption of weakly non-equilibrium state of the plasma. This allowed us to express the solution of the Boltzmann kinetic equation in relaxation time approximation.

We find that the conductivity as a function of the temperature shows a minimum around $0.3T_F$ almost independent of the density and composition of matter, which arises as a result of the transition from the degenerate regime ($T \ll T_F$) to the nondegenerate regime ($T \gg T_F$). Thus, the conductivity decreases with increasing temperature in the degenerate regime up to the point $0.3T_F$; further increase in the temperature leads to a power-law increase in the conductivity as the system enters the non-degenerate regime. We further find that at fixed temperature the conductivity always increases with density, but the slope of the increase is weaker in the non-degenerate regime.

We have further extracted the components of the conductivity tensor in the entire density and temperature range for nonquantizing fields $10^{10} \leq B \leq 10^{14} \text{ G}$. Because the product of relaxation time and cyclotron frequency is a decreasing function of density in the complete temperature

range, low-density matter features anisotropic conductivity at lower magnetic fields. For example, the component of the conductivity transverse to the field $\sigma_0 \rightarrow \sigma$ in the high density limit, but is substantially suppressed at low densities. This underlines the importance of proper inclusion of anisotropy of conductivity in astrophysical studies of dilute magnetized matter even at relatively low magnetic fields.

Our results can be implemented in numerical studies in terms of fit formulas (57)–(63). An alternative is to use plain text tables of conductivities, see Supplemental Material [46].

Finally, our results show that the conductivity depends weakly on the composition of matter. For example, the conductivity of matter composed of heavy elements with $26 \leq Z \leq 36$ in β -equilibrium with electrons differs from the conductivity of matter composed of ^{56}Fe at the same density and temperature by a factor ≤ 1.4 . It would be interesting, however, to study the conductivity of warm multicomponent matter which is composed of nuclei in statistical equilibrium, in which case composition may become an important factor.

ACKNOWLEDGMENTS

We thank L. Rezzolla (L.R.), D. H. Rischke, and J. Schaffner-Bielich for useful discussions, L.R. for drawing our attention to this problem, and M. N. Tamashiro and Y. Levin for useful communications. A.H. acknowledges support from the HGS-HIRe graduate program at Frankfurt University. A.S. is supported by the Deutsche Forschungsgemeinschaft (Grant No. SE 1836/3-1). We acknowledge the support by NewCompStar COST Action MP1304.

APPENDIX A: EVALUATING THE RELAXATION TIME

The purpose of this Appendix is to give the details of the transition from the relaxation time (13) to Eq. (30). We start by defining several angles by the relations $\mathbf{p} \cdot \mathbf{q} = pq \cos \alpha$, $\mathbf{p}_t \cdot \mathbf{p}'_t = p_t p'_t \cos \phi$, and $\mathbf{q} \cdot \mathbf{p}' = qp' \cos \vartheta$, where \mathbf{p}_t , \mathbf{p}'_t are the components of \mathbf{p} , \mathbf{p}' transversal to \mathbf{q} . Writing the second δ -function in Eq. (13) as $\delta(\varepsilon_2 - \varepsilon_4 + \omega) = (M/p'q)\delta(\cos \vartheta - x_0)$, where $x_0 = (2\omega M - q^2)/2p'q$, we find

$$\tau^{-1}(\varepsilon) = \frac{(2\pi)^{-5} M}{p} \int d\omega d\mathbf{q} \cos \alpha \delta(\varepsilon - \varepsilon_3 - \omega) \frac{1 - f_3^0}{1 - f^0} \int_0^\infty dp' p' g(p') S(q) F^2(q) I_\Omega, \quad (\text{A1})$$

where

$$I_\Omega = \int d(\cos \vartheta) d\phi \frac{Z^2 e^{*4}}{2\varepsilon\varepsilon_3} \left[\frac{2\varepsilon^2 - \varepsilon\omega - pq \cos \alpha}{|q^2 + \Pi'_L|^2} + \frac{p^2 \sin^2 \vartheta [2(p \cos \phi)^2 \sin^2 \alpha + (-\varepsilon\omega + qp \cos \alpha)]}{M^2 |q^2 - \omega^2 + \Pi_T|^2} - \frac{2(\varepsilon - \omega)(pp' \sin \alpha \sin \vartheta \cos \phi)}{M \operatorname{Re}(q^2 + \Pi'_L)(q^2 - \omega^2 + \Pi_T^*)} \right] \delta(\cos \vartheta - x_0), \quad (\text{A2})$$

and we substituted the expression for the matrix element (29). After integration over the angle ϕ we obtain

$$I_\Omega = \pi \frac{Z^2 e^{*4}}{\varepsilon(\varepsilon - \omega)} \left[\frac{2\varepsilon^2 - \varepsilon\omega - pq \cos \alpha}{|q^2 + \Pi'_L|^2} + p^2 (1 - x_0^2) \frac{p^2 \sin^2 \alpha + qp \cos \alpha - \varepsilon\omega}{M^2 |q^2 - \omega^2 + \Pi_T|^2} \right] \theta(1 - |x_0|). \quad (\text{A3})$$

The step-function θ defines the minimum value $p'_{\min} = |2\omega M - q^2|/2q$ for the integration over this variable. We substitute Eq. (A3) in Eq. (A1), implement the integration bound on p' and find

$$\tau^{-1}(\varepsilon) = \frac{(2\pi)^{-5} \pi M}{p} \frac{Z^2 e^{*4}}{\varepsilon} \int d\omega d\mathbf{q} \frac{S(q) F^2(q) \cos \alpha}{(\varepsilon - \omega)} \delta(\varepsilon - \varepsilon_3 - \omega) \frac{1 - f_3^0}{1 - f^0} \times \int_{p'_{\min}}^\infty dp' p' g(p') \left[\frac{2\varepsilon^2 - \varepsilon\omega - pq \cos \alpha}{|q^2 + \Pi'_L|^2} + p^2 (1 - x_0^2) \frac{p^2 \sin^2 \alpha + qp \cos \alpha - \varepsilon\omega}{M^2 |q^2 - \omega^2 + \Pi_T|^2} \right]. \quad (\text{A4})$$

The remaining δ function is written as $\delta(\varepsilon - \varepsilon_3 - \omega) = [(\varepsilon - \omega)/pq] \delta(\cos \alpha - y_0) \vartheta(\varepsilon - \omega)$, where $y_0 = (q^2 - \omega^2 + 2\varepsilon\omega)/2pq$. In the next step we integrate over p' to obtain

$$\tau^{-1}(\varepsilon) = \frac{M^2}{8(2\pi)^3 p^3 \beta} \frac{Z^2 e^{*4}}{\varepsilon} \int_{-\infty}^\varepsilon d\omega \frac{1 - f(\varepsilon - \omega)}{1 - f^0(\varepsilon)} \int_0^\infty dq S(q) F^2(q) g(p'_{\min})(q^2 - \omega^2 + 2\varepsilon\omega) \times \theta(1 - |y_0|) \left[\frac{(2\varepsilon - \omega)^2 - q^2}{|q^2 + \Pi'_L|^2} + \frac{1}{\beta M q^2} \frac{(q^2 - \omega^2)[(2\varepsilon - \omega)^2 + q^2] - 4q^2 m^2}{|q^2 - \omega^2 + \Pi_T|^2} \right]. \quad (\text{A5})$$

Finally the θ -function puts some limitations on the integration region over q , specifically $q_- \leq q \leq q_+$, where $q_{\pm} = |\pm \sqrt{\varepsilon^2 - m^2} + \sqrt{(\varepsilon - \omega)^2 - m^2}|$. Note also that to have a real q we need $\omega \leq \varepsilon - m$. Implementing these limits we obtain

$$\begin{aligned} \tau^{-1}(\varepsilon) = & \frac{M^2 T}{8(2\pi)^3 p^3} \frac{Z^2 e^{*4}}{\varepsilon} \int_{-\infty}^{\varepsilon-m} d\omega \frac{1 - f^0(\varepsilon - \omega)}{1 - f^0(\varepsilon)} \int_{q_-}^{q_+} dq S(q) F^2(q) g(p'_{\min})(q^2 - \omega^2 + 2\varepsilon\omega) \\ & \times \left[\frac{(2\varepsilon - \omega)^2 - q^2}{|q^2 + \Pi'_L|^2} + \frac{T}{Mq^2} \frac{(q^2 - \omega^2)[(2\varepsilon - \omega)^2 + q^2] - 4q^2 m^2}{|q^2 - \omega^2 + \Pi_T|^2} \right]. \end{aligned} \quad (\text{A6})$$

Finally we write Eq. (5) as

$$g(p'_{\min}) = n_i \left(\frac{2\pi}{MT} \right)^{3/2} e^{-x^2/2\theta^2} e^{\omega/2T} e^{-q^2/8MT}, \quad (\text{A7})$$

where $x = \omega/q$ and $\theta = \sqrt{T/M}$ and substitute in Eq. (A6) to obtain Eq. (30) of the main text.

In our numerical calculations the temperature varies in the range $0.1 \leq T \leq 10$ MeV and the masses of the nuclei lie in the range from 10^4 MeV to 10^5 MeV. Therefore the parameter θ changes in the range $10^{-3} < \theta < 3 \times 10^{-2} \ll 1$. As a result one can expect that the dynamical part of the scattering amplitude should be suppressed compared with the static part by several orders of magnitude. Numerical calculations show that the contribution of the dynamical part is smaller than 0.15% for ^{12}C and 0.04% for ^{56}Fe and have the order of θ^2 , as expected. Due to the exponent $e^{-x^2/2\theta^2}$ of the expression (A7) only small values of x ($|x| < \theta$) contribute significantly to the integral (30). Therefore, the effective phase volume of the double integration in Eq. (30) reduces to the triangle limited by the lines

$$\omega = \pm\theta q, \quad q_+(\varepsilon, \omega) = 2p - \omega v^{-1} \approx 2p. \quad (\text{A8})$$

as illustrated in Fig. 13. It seen from this figure that the effective width of ω variable is given by $\omega_0 = 2p\theta$.

In Eq. (30) we can take the limit where the ionic component of the plasma is at zero temperature (the temperature of the electronic component is arbitrary so far). Then, because

$$\lim_{\theta \rightarrow 0} \frac{1}{\theta \sqrt{2\pi}} e^{-x^2/2\theta^2} = \delta(x), \quad (\text{A9})$$

we obtain

$$\begin{aligned} \tau^{-1}(\varepsilon) = & \frac{\pi Z^2 e^4 n_i}{\varepsilon p^3} \int_0^{2p} dq q^3 S(q) F^2(q) \\ & \times e^{-q^2/8MT} \frac{4\varepsilon^2 - q^2}{|q^2 + \Pi'_L|^2}, \end{aligned} \quad (\text{A10})$$

where we took into account the fact that for $\omega = 0$ the limits on momentum transfer reduce to $q_- = 0$ and $q_+ = 2p$. Neglecting also the nuclear recoil (which amounts to replacing the exponential factor $e^{-q^2/8MT}$ by unity) we obtain the well-known expression of the relaxation time (32).

Note that the nuclear recoil factor $e^{-q^2/8MT}$ can be important at very low temperatures and high densities for light nuclei, where it can reduce the scattering amplitude significantly. For example, in the extreme case $T = 0.01$ MeV and $\log_{10} \rho = 11$ and ^{12}C we find that the relative error could be larger than a factor of 2. Therefore, Eq. (A10) is a better approximation

than Eq. (32) in the static limit $\omega \rightarrow 0$. However, in the main density-temperature range we consider the nuclear recoil and the dynamical screening introduce only small corrections and do not change the general behavior of the conductivity. The deviations between Eqs. (32) and (30) are smaller than 12% for ^{12}C and 5% for ^{56}Fe .

It can be shown that at densities $\rho < 10^{11}$ g cm $^{-3}$ the effect of nuclear form factor is small as well. Indeed, for the heaviest nucleus that we consider (^{86}Kr) $r_c \simeq 0.025$ MeV $^{-1}$ and the maximal value of the parameter is $qr_c \simeq 0.5$. For small qr_c we can use the approximate formula obtained from Eq. (31)

$$F^2(q) \approx 1 - 0.2(qr_c)^2, \quad (\text{A11})$$

therefore the maximal correction for ^{86}Kr is 5%, which is consistent with numerical results. The corrections are smaller than 4% for ^{56}Fe and 2% for ^{12}C .

Finally we provide in Figs. 14 and 15 numerical values of the relaxation time for a number of cases of interest. We stress that τ is energy-dependent and is evaluated in the degenerate case at the Fermi energy and in the nondegenerate case at $\bar{\varepsilon} \simeq 3T$, which is the thermal energy of ultrarelativistic electrons. In Fig. 14 we show the dependence of the relaxation time

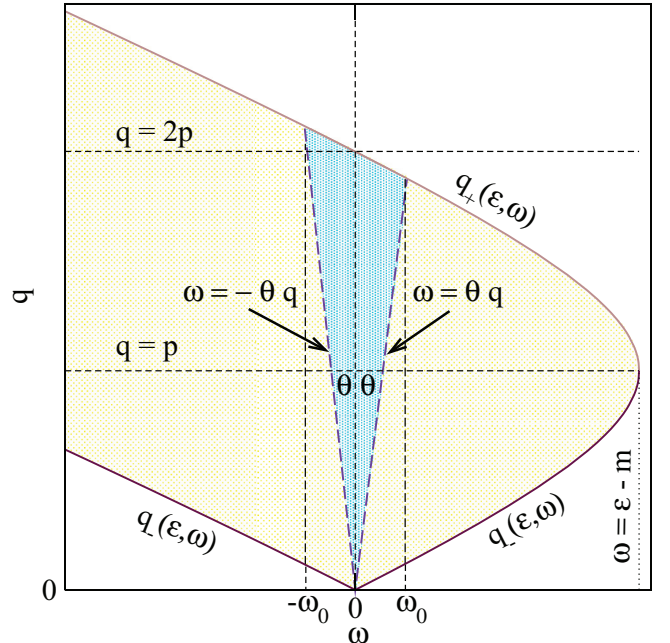


FIG. 13. The integration region in Eq. (30) in the plane (ω, q) (light shaded area) bounded by the functions $q_{\pm}(\varepsilon)$. The major contribution to the integral comes from the triangle bound by the lines $\omega = \pm\theta q$ with the narrow opening angle 2θ (dark shaded area).

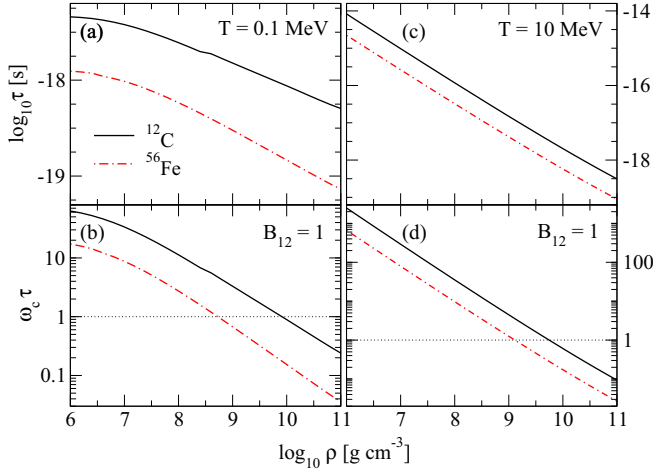


FIG. 14. The relaxation time [(a) and (c)] and dimensionless product $\omega_c \tau$ [(b) and (d)] as functions of density. The temperature is fixed at $T = 0.1$ MeV in (a) and (b) (degenerate regime) and at $T = 10$ MeV in (c) and (d) (nondegenerate regime). The magnetic field is fixed at $B_{12} = 1$.

and the factor $\omega_c \tau$ on density for two values of temperature. It is seen that in the degenerate regime ($T = 0.1$ MeV) the slope of decrease in the relaxation time is smaller than in the case of nondegenerate regime. It is also seen that the factor $\omega_c \tau$ makes a crossover from being much larger than unity at small densities to being much smaller at high densities. This indicates that in low-density matter the effects of anisotropy are much more important than in the high-density matter. In fact, in the nondegenerate case the low-density matter has highly anisotropic conductivity with, for example, $\omega_c \tau \sim 10^3$ for $B_{12} = 1$.

Figure 15 shows the temperature dependence of the relaxation time for several densities. Our results agree well with

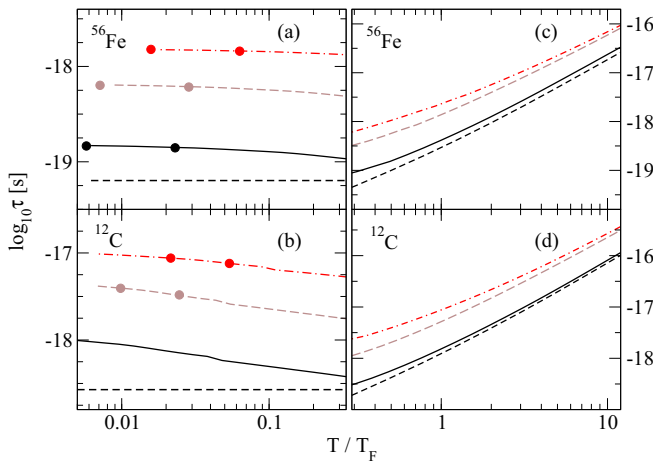


FIG. 15. The relaxation time as a function on dimensionless ratio T/T_F for three values of density: $\log_{10} \rho = 10$ (solid lines), $\log_{10} \rho = 8$ (dashed lines), $\log_{10} \rho = 6$ (dash-dotted lines) for ^{56}Fe [(a) and (c)] and ^{12}C [(b) and (d)]. (a) and (b) correspond to the degenerate and (c) and (d) to the nondegenerate regime. We show the effect of setting $S(q) = 1$ for $\log_{10} \rho = 10$ by short-dashed lines. The open circles reproduce the results of Ref. [15].

those of Nandkumar and Pethick [15] in the degenerate regime. It is seen that τ decreases as a function of temperature in the degenerate regime for $T \leq T^*$ and increases in the nondegenerate regime $T \geq T^*$, which makes clear the existence of the minimum at $T^* = 0.3T_F$ in the conductivity. The temperature decrease in the degenerate regime is caused almost entirely by the structure factor $S(q)$ (see Fig. 15). In the nondegenerate regime the temperature dependence of τ is dominated by the energy increase of electrons with temperature and the role of $S(q)$ is less important, see Fig. 15. This is due to the fact that when $T \geq T_F$, i.e., electrons are nondegenerate, the ionic component forms a Boltzmann gas for composition consisting of ^{56}Fe and ^{12}C nuclei (see Fig. 1).

APPENDIX B: POLARIZATION TENSOR

In this Appendix we outline the derivation of the polarization tensor and the variant of the HTL effective field theory that underlies our computation. Most of the HTL computation are carried out in the ultrarelativistic (massless) limit; here we keep the particle mass nonzero and implement HTL approximation by requiring that the external photon four-momenta are small compared to the fermionic four-momenta within the fermionic loop.

The full photon propagator $D_{\mu\nu}$ can be found from the Dyson equation

$$[D^{-1}]_{\mu\nu} = [D_0^{-1}]_{\mu\nu} - \Pi_{\mu\nu}, \quad (\text{B1})$$

where $D_0^{\mu\nu} = g^{\mu\nu}/Q^2$ is the free photon propagator with $Q^2 = \omega^2 - q^2$. $\Pi_{\mu\nu}$ is the photon polarization tensor and can be decomposed into transverse and longitudinal modes

$$\Pi_{\mu\nu} = \Pi_T P_{\mu\nu}^T + \Pi_L P_{\mu\nu}^L. \quad (\text{B2})$$

We work in the plasma rest frame where the projectors $P_{\mu\nu}^T$ and $P_{\mu\nu}^L$ have the following components:

$$P_{00}^T = 0, \quad P_{0i}^T = 0, \quad P_{ij}^T = -\delta_{ij} + q_i q_j / q^2, \quad (\text{B3})$$

$$P_{00}^L = -q^2/Q^2, \quad P_{0i}^L = -\omega q_i / Q^2, \quad P_{ij}^L = -\frac{\omega^2}{Q^2} \frac{q_i q_j}{q^2}. \quad (\text{B4})$$

They satisfy the relations

$$P_{\mu\alpha}^T P^{T\alpha\nu} = P_{\mu}^{T\nu}, \quad P_{\mu\alpha}^L P^{L\alpha\nu} = P_{\mu}^{L\nu}, \quad P_{\mu\alpha}^T P^{L\alpha\nu} = 0. \quad (\text{B5})$$

From Eqs. (B1)–(B5) it is easy to find the full photon propagator

$$D^{\mu\nu} = \frac{1}{Q^2} \left[g^{\mu\nu} + \frac{\Pi_T}{Q^2 - \Pi_T} P^{T\mu\nu} + \frac{\Pi_L}{Q^2 - \Pi_L} P^{L\mu\nu} \right]. \quad (\text{B6})$$

Using Eq. (B6) and the current conservation law $q^\mu J_\mu = \omega J_0 + q^i J_i = 0$ we can express the scattering amplitude via two scalar functions Π_L and Π_T :

$$\mathcal{M} = J_\mu D^{\mu\nu} J'_\nu = -\frac{J_0 J'_0}{q^2 + \Pi'_L} + \frac{\mathbf{J}_t \mathbf{J}'_t}{q^2 - \omega^2 + \Pi_T}, \quad (\text{B7})$$

where we introduced transversal currents $J_{ii} = J_j(\delta_{ij} - q_i q_j / q^2)$ and $\Pi'_L = -\Pi_L q^2 / Q^2 = \Pi_L / (1 - x^2)$ and $x = \omega / q$. The one-loop diagram in the imaginary-time Matsubara formalism is given by

$$\Pi_{\mu\nu}(\mathbf{q}, \omega_n) = e^{*2} \int \frac{d\mathbf{p}}{(2\pi)^3} T \sum_m \text{Tr}[\gamma_\mu S(\mathbf{p}, \omega_m) \gamma_\nu S(\mathbf{p} - \mathbf{q}, \omega_m - \omega_n)], \quad (\text{B8})$$

where $S(\mathbf{p}, \omega_n)$ is free electron-positron propagator and the sum goes over fermionic (odd) Matsubara frequencies $\omega_m = (2m + 1)\pi T - i\mu$ [$\omega_n = 2n\pi T$ is a bosonic (even) Matsubara frequency]. The propagator $S(\mathbf{p}, \omega_n)$ is given by

$$S(\mathbf{p}, \omega_m) = i \sum_{\pm} \frac{\Lambda_p^{\pm} \gamma_0}{i\omega_m - E_p^{\pm}}, \quad (\text{B9})$$

where Λ_p^{\pm} are the projection operators onto positive and negative energy states

$$\Lambda_p^{\pm} = \frac{\not{p}^{\pm} + m}{2E_p^{\pm}} \gamma_0, \quad p^{\pm} = (E_p^{\pm}, \mathbf{p}) = (\pm E_p, \mathbf{p}). \quad (\text{B10})$$

Substitution of Eq. (B9) into Eq. (B8) gives

$$\Pi_{\mu\nu}(\mathbf{q}, \omega_n) = -e^{*2} \int \frac{d\mathbf{p}}{(2\pi)^3} \sum_{\pm\pm} T \sum_m \frac{\text{Tr}[\gamma_\mu \Lambda_p^{\pm} \gamma_0 \gamma_\nu \Lambda_{p-q}^{\pm} \gamma_0]}{(i\omega_m - E_p^{\pm})(i\omega_m - i\omega_n - E_{p-q}^{\pm})}. \quad (\text{B11})$$

The trace is evaluated using standard field theory methods after substituting therein the projectors (B10):

$$\text{Tr}[\gamma_\mu \Lambda_p^{\pm} \gamma_0 \gamma_\nu \Lambda_{p-q}^{\pm} \gamma_0] = \frac{p_\mu^{\pm} p_\nu^{\pm} + p_\nu^{\pm} p_\mu^{\pm} - g_{\mu\nu}[(p^{\pm} p^{\pm}) - m^2]}{E_p^{\pm} E_{p-q}^{\pm}}, \quad \mathbf{p}' = \mathbf{p} - \mathbf{q}. \quad (\text{B12})$$

The summation over the Matsubara frequencies gives

$$T \sum_m \frac{1}{(i\omega_m - E_p^{\pm})(i\omega_m - i\omega_n - E_{p-q}^{\pm})} = \frac{f^+(E_p^{\pm}) - f^+(E_{p-q}^{\pm})}{E_p^{\pm} - E_{p-q}^{\pm} - i\omega_n}, \quad (\text{B13})$$

where $f^{\pm}(E) = [e^{\beta(E \mp \mu)} + 1]^{-1}$ (note that in the main text we use f^0 instead of f^+). Substituting Eqs. (B12) and (B13) into Eq. (B11) we obtain

$$\Pi_{\mu\nu}(\mathbf{q}, \omega_n) = -e^{*2} \int \frac{d\mathbf{p}}{(2\pi)^3} \sum_{\pm\pm} \frac{p_\mu^{\pm} p_\nu^{\pm} + p_\nu^{\pm} p_\mu^{\pm} - g_{\mu\nu}[(p^{\pm} p^{\pm}) - m^2]}{E_p^{\pm} E_{p-q}^{\pm}} \frac{f^+(E_p^{\pm}) - f^+(E_{p-q}^{\pm})}{E_p^{\pm} - E_{p-q}^{\pm} - i\omega_n}. \quad (\text{B14})$$

Consider the spatial components of Eq. (B14)

$$\begin{aligned} \Pi_{ij} = & -e^{*2} \int \frac{d\mathbf{p}}{(2\pi)^3} \left\{ \frac{p_i p'_j + p_j p'_i - \delta_{ij}(m^2 - E_p E_{p-q} + \mathbf{p} \cdot \mathbf{p}')}{E_p E_{p-q}} \left[\frac{f^+(E_p) - f^+(E_{p-q})}{E_p - E_{p-q} - i\omega_n} + \frac{f^+(-E_p) - f^+(-E_{p-q})}{-E_p + E_{p-q} - i\omega_n} \right] \right. \\ & \left. - \frac{p_i p'_j + p_j p'_i - \delta_{ij}(m^2 + E_p E_{p-q} + \mathbf{p} \cdot \mathbf{p}')}{E_p E_{p-q}} \left[\frac{f^+(E_p) - f^+(-E_{p-q})}{E_p + E_{p-q} - i\omega_n} + \frac{f^+(-E_p) - f^+(E_{p-q})}{-E_p - E_{p-q} - i\omega_n} \right] \right\}. \quad (\text{B15}) \end{aligned}$$

The part of the polarization tensor $\propto \delta_{ij}$ gives

$$\begin{aligned} \Pi_{ij}^{(1)}(\mathbf{q}, \omega_n) = & -e^{*2} \delta_{ij} \int \frac{d\mathbf{p}}{(2\pi)^3} \left\{ -\frac{m^2 - E_p E_{p-q} + \mathbf{p} \cdot \mathbf{p}'}{E_p E_{p-q}} \left[\frac{f^+(E_p) - f^+(E_{p-q})}{E_p - E_{p-q} - i\omega_n} + \frac{f^+(-E_p) - f^+(-E_{p-q})}{-E_p + E_{p-q} - i\omega_n} \right] \right. \\ & \left. + \frac{m^2 + E_p E_{p-q} + \mathbf{p} \cdot \mathbf{p}'}{E_p E_{p-q}} \left[\frac{f^+(E_p) - f^+(-E_{p-q})}{E_p + E_{p-q} - i\omega_n} + \frac{f^+(-E_p) - f^+(E_{p-q})}{-E_p - E_{p-q} - i\omega_n} \right] \right\}. \quad (\text{B16}) \end{aligned}$$

In the spirit of the HTL approximation we next put $\mathbf{q} = 0$ in the prefactors multiplying the occupation numbers, use the relation $f^+(-E) = 1 - f^-(E)$ and drop the vacuum contributions $\propto 1$ to obtain

$$\Pi_{ij}^{(1)}(\mathbf{q}, \omega_n) = -2e^{*2} \delta_{ij} \int \frac{d\mathbf{p}}{(2\pi)^3} \left[\frac{f^+(E_p) + f^-(E_p)}{E_p} \right]. \quad (\text{B17})$$

In the remaining part of the polarization tensor we set $(p_i p'_j + p_j p'_i)/(E_p E_{p-q}) \simeq 2p_i p_j/E_p^2$ to find

$$\begin{aligned} \Pi_{ij}^{(2)}(\mathbf{q}, \omega_n) = & -2e^{*2} \int \frac{d\mathbf{p}}{(2\pi)^3} \frac{p_i p_j}{E_p^2} \left\{ \left[\frac{f^+(E_p) - f^+(E_{p-q})}{E_p - E_{p-q} - i\omega_n} + \frac{f^+(-E_p) - f^+(-E_{p-q})}{-E_p + E_{p-q} - i\omega_n} \right] \right. \\ & \left. - \left[\frac{f^+(E_p) - f^+(-E_{p-q})}{E_p + E_{p-q} - i\omega_n} + \frac{f^+(-E_p) - f^+(E_{p-q})}{-E_p - E_{p-q} - i\omega_n} \right] \right\}. \end{aligned} \quad (\text{B18})$$

We further approximate

$$E_{p-q} = E_p - \frac{(\mathbf{p} \cdot \mathbf{q})}{E_p}, \quad (\text{B19})$$

$$f^+(E_p) - f^+(E_{p-q}) = \frac{(\mathbf{p} \cdot \mathbf{q})}{E_p} \frac{\partial f^+(E_p)}{\partial E_p}, \quad (\text{B20})$$

$$f^+(-E_p) - f^+(-E_{p-q}) = -\frac{(\mathbf{p} \cdot \mathbf{q})}{E_p} \frac{\partial f^-(E_p)}{\partial E_p}, \quad (\text{B21})$$

and drop the vacuum terms to obtain

$$\begin{aligned} \Pi_{ij}^{(2)}(\mathbf{q}, \omega_n) = & -2e^{*2} \int \frac{d\mathbf{p}}{(2\pi)^3} \frac{p_i p_j}{E_p^2} \left\{ \left[\frac{\partial f^+(E_p)}{\partial E_p} + \frac{\partial f^-(E_p)}{\partial E_p} \right] \right. \\ & \left. + \frac{i\omega E_p}{(\mathbf{p} \cdot \mathbf{q}) - i\omega_n E_p} \left[\frac{\partial f^+(E_p)}{\partial E_p} + \frac{\partial f^-(E_p)}{\partial E_p} \right] - \frac{f^+(E_p) + f^-(E_p)}{E_p} \right\}. \end{aligned} \quad (\text{B22})$$

Now we add Eq. (B17) to this to obtain

$$\begin{aligned} \Pi_{ij}(\mathbf{q}, \omega_n) = & -2e^{*2} \int \frac{p^2 dp}{2\pi^2} \int \frac{d\Omega}{4\pi} \left\{ \delta_{ij} \left[\frac{f^+(E_p) + f^-(E_p)}{E_p} \right] - \frac{p_i p_j}{E_p^2} \left[\frac{f^+(E_p) + f^-(E_p)}{E_p} \right] \right. \\ & \left. + \frac{p_i p_j}{E_p^2} \left[\frac{\partial f^+(E_p)}{\partial E_p} + \frac{\partial f^-(E_p)}{\partial E_p} \right] - \frac{p_i p_j}{E_p^2} \frac{i\omega E_p}{i\omega_n E_p - (\mathbf{p} \cdot \mathbf{q})} \left[\frac{\partial f^+(E_p)}{\partial E_p} + \frac{\partial f^-(E_p)}{\partial E_p} \right] \right\}. \end{aligned} \quad (\text{B23})$$

In the first three terms in Eq. (B23) the angular and radial integrals separate. For the angular part we have

$$\int \frac{d\Omega}{4\pi} \frac{p_i p_j}{p^2} = \frac{\delta_{ij}}{3}. \quad (\text{B24})$$

By partial integration we find

$$\int d\varepsilon \frac{p^3}{\varepsilon} \frac{d}{d\varepsilon} [f^+(\varepsilon) + f^-(\varepsilon)] = -3 \int [f^+(\varepsilon) + f^-(\varepsilon)] \left(1 - \frac{p^2}{3\varepsilon^2}\right) p d\varepsilon \quad (\text{B25})$$

which implies that the sum of these terms vanishes. For the remainder we find

$$\Pi_{ij}(\mathbf{q}, \omega) = \frac{4e^2}{\pi} \int p^2 dp \left[\frac{\partial f^+(E_p)}{\partial E_p} + \frac{\partial f^-(E_p)}{\partial E_p} \right] v^2 \int \frac{d\Omega}{4\pi} n_i n_j \frac{\omega}{\omega + i\delta - v(\mathbf{n} \cdot \mathbf{q})}, \quad (\text{B26})$$

where $v = (\partial E_p / \partial p) = p/E_p$ and in the last term we have performed the analytical continuation $i\omega_n \rightarrow \omega + i\delta$. The spatial part of the polarization tensor can be decomposed as

$$\Pi_{ij}(\mathbf{q}, \omega) = P_{ij}^T \Pi_T(\mathbf{q}, \omega) + P_{ij}^L \Pi_L(\mathbf{q}, \omega). \quad (\text{B27})$$

Contracting Eq. (B27) with δ_{ij} and using Eqs. (B3) and (B4) we find

$$2\Pi_T(\mathbf{q}, \omega) + \frac{\omega^2}{\omega^2 - q^2} \Pi_L(\mathbf{q}, \omega) = \left(-\frac{4e^2}{\pi}\right) \int p^2 dp \left[\frac{\partial f^+(E_p)}{\partial E_p} + \frac{\partial f^-(E_p)}{\partial E_p} \right] v^2 L_v(\mathbf{q}, \omega), \quad (\text{B28})$$

where

$$L_v(\mathbf{q}, \omega) \equiv \int \frac{d\Omega}{4\pi} \frac{\omega}{\omega + i\delta - v(\mathbf{n} \cdot \mathbf{q})} = \frac{x}{2v} \log \frac{x+v}{x-v}, \quad x \equiv \omega/q. \quad (\text{B29})$$

Next contract Eq. (B27) with $q_i q_j$ to find (note that $q_i q_j P_{ij}^T = 0$)

$$\frac{q^2}{\omega^2 - q^2} \Pi^L(\mathbf{q}, \omega) = \left(-\frac{4e^2}{\pi}\right) \int p^2 dp \left[\frac{\partial f^+(E_p)}{\partial E_p} + \frac{\partial f^-(E_p)}{\partial E_p} \right] [L_v(\mathbf{q}, \omega) - 1]. \quad (\text{B30})$$

Using Eqs. (B28)–(B30) we obtain Eqs. (40) and (41) of the main text.

- [1] L. Mestel and F. Hoyle, On the thermal conductivity in dense stars, *Proc. Cambridge Philos. Soc.* **46**, 331 (1950).
- [2] T. D. Lee, Hydrogen content and energy-productive mechanism of white dwarfs, *Astrophys. J.* **111**, 625 (1950).
- [3] A. A. Abrikosov, The conductivity of strongly compressed matter, *Sov. Phys. JETP* **18**, 1399 (1964).
- [4] W. B. Hubbard, Studies in stellar evolution. V. Transport coefficients of degenerate stellar matter, *Astrophys. J.* **146**, 858 (1966).
- [5] M. Lampe, Transport coefficients of degenerate plasma, *Phys. Rev.* **170**, 306 (1968).
- [6] L. Mestel and M. A. Ruderman, The energy content of a white dwarf and its rate of cooling, *MNRAS* **136**, 27 (1967).
- [7] I. Iben, Jr., Electron conduction in red giants, *Astrophys. J.* **154**, 557 (1968).
- [8] M. Lampe, Transport theory of a partially degenerate plasma, *Phys. Rev.* **174**, 276 (1968).
- [9] W. B. Hubbard and M. Lampe, Thermal conduction by electrons in stellar matter, *Astrophys. J. Suppl. Ser.* **18**, 297 (1969).
- [10] A. B. Solinger, Electrical and thermal conductivity in a superdense lattice. I. High-temperature conductivity, *Astrophys. J.* **161**, 553 (1970).
- [11] V. Canuto, Electrical conductivity and conductive opacity of a relativistic electron gas, *Astrophys. J.* **159**, 641 (1970).
- [12] A. Kovetz and G. Shaviv, The electrical and thermal conductivities of stellar degenerate matter, *A&A* **28**, 315 (1973).
- [13] E. Flowers and N. Itoh, Transport properties of dense matter, *Astrophys. J.* **206**, 218 (1976).
- [14] D. G. Yakovlev and V. A. Urpin, Thermal and electrical conductivity in white dwarfs and neutron stars, *Soviet Ast.* **24**, 303 (1980).
- [15] R. Nandkumar and C. J. Pethick, Transport coefficients of dense matter in the liquid metal regime, *MNRAS* **209**, 511 (1984).
- [16] I. Easson and C. J. Pethick, Magnetohydrodynamics of neutron star interiors, *Astrophys. J.* **227**, 995 (1979).
- [17] N. Itoh, S. Mitake, H. Iyetomi, and S. Ichimaru, Electrical and thermal conductivities of dense matter in the liquid metal phase. I - High-temperature results, *Astrophys. J.* **273**, 774 (1983).
- [18] N. Itoh, Y. Kohyama, N. Matsumoto, and M. Seki, Electrical and thermal conductivities of dense matter in the crystalline lattice phase, *Astrophys. J.* **285**, 758 (1984).
- [19] S. Mitake, S. Ichimaru, and N. Itoh, Electrical and thermal conductivities of dense matter in the liquid metal phase. II - Low-temperature quantum corrections, *Astrophys. J.* **277**, 375 (1984).
- [20] D. M. Sedrakyan and A. K. Avetisyan, Magneto-hydrodynamics of plasma in the crust of a neutron star, *Astrophys.* **26**, 295 (1987).
- [21] N. Itoh and Y. Kohyama, Electrical and thermal conductivities of dense matter in the crystalline lattice phase. II - Impurity scattering, *Astrophys. J.* **404**, 268 (1993).
- [22] N. Itoh, H. Hayashi, and Y. Kohyama, Electrical and thermal conductivities of dense matter in the crystalline lattice phase. III. Inclusion of lower densities, *Astrophys. J.* **418**, 405 (1993).
- [23] D. A. Baiko, A. D. Kaminker, A. Y. Potekhin, and D. G. Yakovlev, Ion Structure Factors and Electron Transport in Dense Coulomb Plasmas, *Phys. Rev. Lett.* **81**, 5556 (1998).
- [24] A. Y. Potekhin, D. A. Baiko, P. Haensel, and D. G. Yakovlev, Transport properties of degenerate electrons in neutron star envelopes and white dwarf cores, *A&A* **346**, 345 (1999).
- [25] N. Itoh, S. Uchida, Y. Sakamoto, Y. Kohyama, and S. Nozawa, The second born corrections to the electrical and thermal conductivities of dense matter in the liquid metal phase, *Astrophys. J.* **677**, 495 (2008).
- [26] C. J. Horowitz, D. K. Berry, C. M. Briggs, M. E. Caplan, A. Cumming, and A. S. Schneider, Disordered Nuclear Pasta, Magnetic Field Decay, and Crust Cooling in Neutron Stars, *Phys. Rev. Lett.* **114**, 031102 (2015).
- [27] A. Y. Potekhin, Electron conduction in magnetized neutron star envelopes, *A&A* **351**, 787 (1999).
- [28] C. Palenzuela, L. Lehner, O. Reula, and L. Rezzolla, Beyond ideal MHD: Towards a more realistic modeling of relativistic astrophysical plasmas, *MNRAS* **394**, 1727 (2009).
- [29] K. Dionysopoulou, D. Alic, C. Palenzuela, L. Rezzolla, and B. Giacomazzo, General-relativistic resistive magnetohydrodynamics in three dimensions: Formulation and tests, *Phys. Rev. D* **88**, 044020 (2013).
- [30] C. Palenzuela, L. Lehner, S. L. Liebling, M. Ponce, M. Anderson, D. Neilsen, and P. Motl, Linking electromagnetic and gravitational radiation in coalescing binary neutron stars, *Phys. Rev. D* **88**, 043011 (2013).
- [31] K. Dionysopoulou, D. Alic, and L. Rezzolla, General-relativistic resistive-magnetohydrodynamic simulations of binary neutron stars, *Phys. Rev. D* **92**, 084064 (2015).
- [32] J. M. Pearson, S. Goriely, and N. Chamel, Properties of the outer crust of neutron stars from Hartree-Fock-Bogoliubov mass models, *Phys. Rev. C* **83**, 065810 (2011).
- [33] H. Heiselberg and C. J. Pethick, Transport and relaxation in degenerate quark plasmas, *Phys. Rev. D* **48**, 2916 (1993).
- [34] M. G. Alford, H. Nishimura, and A. Sedrakian, Transport coefficients of two-flavor superconducting quark matter, *Phys. Rev. C* **90**, 055205 (2014).
- [35] S. Galam and J.-P. Hansen, Statistical mechanics of dense ionized matter. VI. Electron screening corrections to the thermodynamic properties of the one-component plasma, *Phys. Rev. A* **14**, 816 (1976).
- [36] M. N. Tamashiro, Y. Levin, and M. C. Barbosa, The one-component plasma: A conceptual approach, *Physica A* **268**, 24 (1999).
- [37] E. Braaten and R. D. Pisarski, Soft amplitudes in hot gauge theories: A general analysis, *Nucl. Phys. B* **337**, 569 (1990).
- [38] E. Braaten and R. D. Pisarski, Deducing hard thermal loops from Ward identities, *Nucl. Phys. B* **339**, 310 (1990).
- [39] T. Altherr and U. Kraemmer, Gauge field theory methods for ultra-degenerate and ultra-relativistic plasmas, *Astropart. Phys.* **1**, 133 (1992).
- [40] T. Altherr, E. Petitgirard, and T. D. R. Gaztelurrutia, Photon propagation in dense media, *Astropart. Phys.* **1**, 289 (1993).
- [41] T. Altherr, E. Petitgirard, and T. del Río Gaztelurrutia, Axion emission from red giants and white dwarfs, *Astropart. Phys.* **2**, 175 (1994).
- [42] R. N. Wolf, D. Beck, K. Blaum, C. Böhm, C. Borgmann, M. Breitenfeldt *et al.*, Plumbing Neutron Stars to New Depths with

- the Binding Energy of the Exotic Nuclide Zn82, *Phys. Rev. Lett.* **110**, 041101 (2013).
- [43] G. Baym, C. Pethick, and P. Sutherland, The ground state of matter at high densities: Equation of state and stellar models, *Astrophys. J.* **170**, 299 (1971).
- [44] S. L. Shapiro and S. A. Teukolsky, *Black Holes, White Dwarfs and Neutron Stars: The Physics of Compact Objects* (Wiley, New York, 1986).
- [45] S. B. Rüster, M. Hempel, and J. Schaffner-Bielich, Outer crust of nonaccreting cold neutron stars, *Phys. Rev. C* **73**, 035804 (2006).
- [46] See Supplemental Material at <http://link.aps.org/supplemental/10.1103/PhysRevC.94.025805> for density and temperature dependent components of conductivity tensor for fixed magnetic fields $B_{12} = 1, 10, 100$ and for matter composed of ^{56}Fe , ^{12}C and in β -equilibrium.